3. **Bibevski S and Dunlap ME.** Prevention of diminished parasympathetic control of the heart in experimental heart failure. *Am J Physiol Heart Circ Physiol* 287: H1780–H1785, 2004.
4. **Brookes PS, Yoon Y, Robotham JL, Anders MW, and Sheu SS.** Calcium, ATP, and ROS: a mitochondrial love-hate triangle. *Am J Physiol Cell Physiol* 287: C817–C833, 2004.
5. **Caldwell RA, Clemo HF, and Baumgarten CM.** Using gadolinium to identify stretch-activated channels: technical considerations. *Am J Physiol Cell Physiol* 275: C619–C621, 1998.
6. **Glantz SA.** *Primer of Biostatistics* (5th ed) New York: McGraw-Hill, 2002.
7. **Hirche HJ, Franz CHR, Bös L, Bissig R, Lang R, and Schramm M.** Myocardial extracellular K^+ and H^+ increase and noradrenaline release as possible cause of early arrhythmias following acute coronary artery occlusion in pigs. *J Mol Cell Cardiol* 12: 579–593, 1979.
8. **Hong SJ and Chang CC.** Calcium channel subtypes for the sympathetic and parasympathetic nerves of guinea-pig atria. *Br J Pharmacol* 116: 1577–1582, 1995.
9. **Iwamoto T, Kita S, Uehara A, Inoue Y, Taniguchi Y, Imanaga I, and Shigekawa M.** Structural domains influencing sensitivity to isothiourea derivative inhibitor KB-R7943 in cardiac Na^+/Ca^{2+} exchanger. *Mol Pharmacol* 59: 524–531, 2001.
10. **Iwamoto T, Watano T, and Shigekawa M.** A novel isothiourea derivative selectively inhibits the reverse mode of Na^+/Ca^{2+} exchange in cells expressing NCX1. *J Biol Chem* 271: 22391–22397, 1996.
11. **Johnson TA, Gray AL, Lauenstein JM, Newton SS, and Massari VJ.** Parasympathetic control of the heart. I. An interventriculo-septal ganglion is the major source of the vagal intracardiac innervation of the ventricles. *J Appl Physiol* 96: 2265–2272, 2004.
12. **Kawada T, Yamazaki T, Akiyama T, Inagaki M, Shishido T, Zheng C, Yanagiya Y, Sugimachi M, and Sunagawa K.** Vagosympathetic interactions in ischemia-induced myocardial norepinephrine and acetylcholine release. *Am J Physiol Heart Circ Physiol* 280: H216–H221, 2001.
13. **Kawada T, Yamazaki T, Akiyama T, Li M, Ariumi H, Mori H, Sunagawa K, and Sugimachi M.** Vagal stimulation suppresses ischemia-induced myocardial interstitial norepinephrine release. *Life Sci* 78: 882–887, 2006.
14. **Kawada T, Yamazaki T, Akiyama T, Sato T, Shishido T, Inagaki M, Takaki H, Sugimachi M, and Sunagawa K.** Differential acetylcholine release mechanisms in the ischemic and non-ischemic myocardium. *J Mol Cell Cardiol* 32: 405–414, 2000.
15. **Kawada T, Yamazaki T, Akiyama T, Shishido T, Inagaki M, Uemura K, Miyamoto T, Sugimachi M, Takaki H, and Sunagawa K.** In vivo assessment of acetylcholine-releasing function at cardiac vagal nerve terminals. *Am J Physiol Heart Circ Physiol* 281: H139–H145, 2001.
16. **Kimura J, Watano T, Kawahara M, Sakai E, and Yatabe J.** Direction-independent block of bi-directional Na^+/Ca^{2+} exchange current by KB-R7943 in guinea-ping cardiac myocytes. *Br J Pharmacol* 128: 969–974, 1999.
17. **Kimura S, Mieno H, Tamaki K, Inoue M, and Chayama K.** Nonselective cation channel as a Ca^{2+} influx pathway in pepsinogen-secreting cells of bullfrog esophagus. *Am J Physiol Gastrointest Liver Physiol* 281: G333–G341, 2001.
18. **Kléber AG.** Extracellular potassium accumulation in acute myocardial ischemia. *J Mol Cell Cardiol* 16: 389–394, 1984.
19. **Kurokawa J, Adachi-Akahane S, and Nagao T.** 1-5-Benzothiazepine binding domain is located on the extracellular side of the cardiac L-type Ca^{2+} channel. *Mol Pharmacol* 51: 262–268, 1997.
20. **Lazdunski M, Frelin C, and Vigne P.** The sodium/hydrogen exchange system in cardiac cells: its biochemical and pharmacological properties and its role in regulating internal concentrations of sodium and internal pH. *J Mol Cell Cardiol* 17: 1029–1042, 1985.
21. **Lee C, Dhalla NS, and Hryshko LV.** Therapeutic potential of novel Na^+-Ca^{2+} exchange inhibitors in attenuating ischemia-reperfusion injury. *Can J Cardiol* 21: 509–516, 2005.
22. **Li M, Zheng C, Sato T, Kawada T, Sugimachi M, and Sunagawa K.** Vagal nerve stimulation markedly improves long-term survival after chronic heart failure in rats. *Circulation* 109: 120–124, 2004.
23. **Molderings GJ, Likungu J, and Göthert M.** N-type calcium channels control sympathetic neurotransmission in human heart atrium. *Circulation* 101: 403–407, 2000.
24. **Nicholls DG.** *Proteins, Transmitters and Synapses*. Oxford: Blackwell Science, 1994.
25. **Oka T, Sato K, Hori M, Ozaki H, and Karaki H.** Xestospongin C, a novel blocker of IP_3 receptor, attenuates the increase in cytosolic calcium level and degranulation that is induced by antigen in RBL-2H3 mast cells. *Br J Pharmacol* 135: 1959–1966, 2002.
26. **Randall A and Tsien RW.** Pharmacological dissection of multiple types of Ca^{2+} channel currents in rat cerebellar granule neurons. *J Neurosci* 15: 2995–3012, 1995.
27. **Schauerte P, Scherlag BJ, Scherlag MA, Goli S, Jackman WM, and Lazzara R.** Ventricular rate control during atrial fibrillation by cardiac parasympathetic nerve stimulation: a transvenous approach. *J Am Coll Cardiol* 34: 2043–2050, 1999.
28. **Serone AP and Angus JA.** Role of N-type calcium channels in autonomic neurotransmission in guinea-pig isolated left atria. *Br J Pharmacol* 127: 927–934, 1999.
29. **Smith AB, Motin L, Lavidis NA, and Adams DJ.** Calcium channels controlling acetylcholine release from preganglionic nerve terminals in rat autonomic ganglia. *Neuroscience* 95: 1121–1127, 2000.
30. **Verkhratsky A and Toescu EC.** Endoplasmic reticulum Ca^{2+} homeostasis and neuronal death. *J Cell Mol Med* 4: 351–361, 2003.
31. **Waterman SA.** Multiple subtypes of voltage-gated calcium channel mediate transmitter release from parasympathetic neurons in the mouse bladder. *J Neurosci* 16: 4155–4161, 1996.
32. **Wheeler DB, Randall A, and Tsien RW.** Changes in action potential duration after reliance of excitatory synaptic transmission on multiple types of Ca^{2+} channels in rat hippocampus. *J Neurosci* 16: 2226–2237, 1996.
33. **Yahagi N, Akiyama T, and Yamazaki T.** Effects of ω-conotoxin GVIA on cardiac sympathetic nerve function. *J Auton Nerv Syst* 68: 43–48, 1998.
34. **Yamazaki T, Akiyama T, Kitagawa H, Takauchi Y, Kawada T, and Sunagawa K.** A new, concise dialysis approach to assessment of cardiac sympathetic nerve terminal abnormalities. *Am J Physiol Heart Circ Physiol* 272: H1182–H1187, 1997.
35. **Yoshitomi O, Akiyama D, Hara T, Cho S, Tomiyasu S, and Sumikawa K.** Cardioprotective effects of KB-R7943, a novel inhibitor of Na^+/Ca^{2+} exchanger, on stunned myocardium in anesthetized dogs. *J Anesth* 19: 124–130, 2005.
36. **Zhang JF, Randall AD, Ellinor PT, Horne WA, Sather WA, Tanabe T, Schwarz TL, and Tsien RW.** Distinctive pharmacology and kinetics of cloned neuronal Ca^{2+} channels and their possible counterparts in mammalian CNS neurons. *Neuropharmacology* 32: 1075–1088, 1993.

J. Clin. Biochem. Nutr., 38, 95–102, March 2006

Biphasic Action of Inducible Nitric Oxide Synthase in a Hindlimb Ischemia Model

Koji Kimura[1], Takako Goto[1], Kentarou Yagi[1], Hidekazu Furuya[1], Shio Jujo[2], Johbu Itoh[3], Sadaaki Sawamura[4], Shirosaku Koide[1], Hidezo Mori[5,*], and Naoto Fukuyama[2,*]

[1]*Department of Surgery, Division of Cardiovascular Surgery, School of Medicine, Tokai University, Kanagawa 259-1193, Japan*
[2]*Department of Physiology School of Medicine, Tokai University, Kanagawa 259-1193, Japan*
[3]*Department of Pathology School of Medicine, Tokai University, Kanagawa 259-1193, Japan*
[4]*Department of Microbiology, School of Medicine, Tokai University, Kanagawa 259-1193, Japan*
[5]*Department of Cardiac Physiology, National Cardiovascular Center, Osaka 565-8565, Japan*

Received 17 October, 2005; Accepted 22 November, 2005

Summary We investigated the influence of inducible nitric oxide synthase (iNOS) on acute ischemic injury and chronic angiogenesis. In a hindlimb ischemia model, NO produced by endothelial NO synthase (eNOS) reduces ischemic injury and promotes angiogenesis. However, the effect of the large amounts of NO generated by induced iNOS is unclear. Experimental groups of mice were as follows: (1) wild-type group (Wild), (2) iNOS-knockout group (iNOS-KO), and (3) aminoguanidine-treated wild-type group (Wild + AG), which received aminoguanidine from day 0 to day 3 after ischemia. Acute ischemic injury was evaluated by measuring the plasma CK value and ischemic score. Chronic angiogenesis was evaluated by microangiography and with a non-contact type Doppler blood flowmeter on day 3. Compared with the Wild group (251 ± 34.7 IU/l), the CK value was significantly elevated in the iNOS-KO (497 ± 126.7 IU/l) and Wild + AG (587.2 ± 128.7 IU/l) groups. The ischemic score was significantly increased in the iNOS-KO (92%) and Wild ± AG (66.6%) groups compared with the Wild group (23%). Blood flow was significantly increased in the iNOS-KO group (58.7 ± 15.3%) compared with the Wild (38.1 ± 15.9%) and Wild ± AG (43.5 ± 9.8%) groups in the chronic stage. Microangiography revealed a significantly increased number of blood vessels in the iNOS-KO (0.29 ± 0.02) group compared with the Wild (0.12 ± 0.01) and Wild + AG (0.15 ± 0.02) groups. Our findings indicate that NO generated by iNOS has a biphasic action, reducing acute ischemic injury and inhibiting angiogenesis in the chronic stage.

Key Words: angiogenesis, ischemia, nitric oxide synthase

Introduction

The incidence of refractory peripheral arterial disease is increasing rapidly in developed countries [*1*]. When peripheral arterial disease becomes severe, not only is the quality of life of patients impaired, but also their prognosis is poor [*2*]. Consequently new therapies, including angiogenic treatment with vascular endothelial growth factor (VEGF), hepatocyte growth factor (HGF) and fibroblast growth factor-4 (FGF-4) gene transduction or bone marrow cells, have been developed, with some success [*3-8*].

NO is produced by NO synthase and has multiple bioactivities, including vasodilating, anti-platelet-aggregating

*To whom correspondence should be addressed.
Tel: +81-463-931-121 Fax: +81-463-936-684
E-mail: fukuyama@is.icc.u-tokai.ac.jp

and anti-microbial activities [*9*]. Among the three NO synthase isoforms, neuronal NO synthase (nNOS) is found in the central nerve system, and iNOS is induced in smooth-muscle cells and inflammatory cells in various diseases, such as endotoxemia or ischemia, while eNOS is found in vascular endothelial cells [*10*].

NO generally has a cytoprotective action on hindlimb ischemia [*11–14*]. During ischemic injury, eNOS is upregulated and iNOS is induced. It is reasonable that NO produced by eNOS reduces acute ischemic injury and induces angiogenesis, as it has been shown to have a vasodilatory action [*15–17*]. Induced iNOS produces large amounts of NO [*18*], but the effect of NO generated by iNOS in hindlimb ischemia remains unclear.

In this experiment, we examined the contributions of iNOS to the acute phase of ischemic injury and to angiogenesis in the chronic phase of ischemia in a mouse hindlimb ischemia model, using iNOS knockout mice and wild-type mice treated with aminoguanidine (a selective inhibitor of inducible nitric oxide synthese in macrophages)[*19–21*] in the acute phase.

Materials and Methods

Mice

All mice used in experiments were male, 2 to 3 months of age, weighing 18 to 26 g each. Wild-type (Wild) 129 SvEv mice were purchased from CLEA, Japan. iNOS –/– mice, with a mixed C57BL/6J × 129 SvEv genetic background, were obtained from Merck & Co, Inc.. INOS +/+ mice were obtained by crossing 129 SvEv mice with C57BL/6J mice twice. INOS –/– and iNOS +/+ strains have similar genetic backgrounds of 75% C57BL/6J and 25% 129/SvEv [*22*]. For the pharmacologically iNOS-inhibited group, Wild mice were given aminoguanidine (AG; Sigma, 50 mg/kg, i.p., KI value of 55 micro M and a $K_{inact\ max}$ value of 0.09 min^{-1}) [*23*] 24 hr before operation and daily for 3 days postoperatively [*24, 25*]. The animals were maintained in a pathogen-free barrier facility with a 12-hour light/dark cycle and had free access to food and water. Animals were anesthetized with pentobarbital sodium (50 mg/kg, i.p.), and hindlimb ischemia was created by ligation of the left common iliac artery and external iliac artery and resection of the femoral artery [*26, 27*]. Mice were killed 7 days (acute phase) or 14 to 21 days (chronic phase) after surgery [*28*]. The study was approved by the Animal Care Committee of Tokai University.

Evaluation of acute ischemic injury

Serum CK value—To estimate skeletal muscle injury, CK release was estimated in the effluent collected from the infraorbitalis vein on day 3. Plasma was obtained through centrifugation of the whole blood for 10 minutes at 12000 g at 4°C. Plasma was collected and CK was assayed by SRL Co..

Ischemic score—On day 7, the degree of ischemic insult in the limb was macroscopically evaluated by using graded morphological scales for tissue necrosis (grade 0 to IV): grade 0: absence of necrosis: grade I, necrosis only of toes; grade II, necrosis extending to dorsum of a foot; grade III, necrosis extending to crus; grade IV, necrosis extending to a thigh or complete necrosis (Fig. 1).

Evaluation of chronic angiogenesis

Non-contact type laser Doppler measurement—We employed laser Doppler flowmetry (LDF), a non-nvasive technique for measuring tissue blood flow [*16, 29*], using a FLO-N1 device (OMEGAWAVE, Japan), which delivers light generated by a semiconductor laser diode operating at a wavelength of 780 nm, with a maximum accessible power of 3 mW. Briefly, the skin was removed so that only deep muscle blood flow would be measured, and the probe (ST-N probe, OMEGAWAVE, Japan) was placed on 4 points of the femoral muscles. Blood flow was expressed as ml/min/100 g. The contralateral hindlimb served as an internal control.

Sequential microangiography in in vivo—A PE-10 (10-gauge polyethylene) catheter was placed in the right common carotid artery of a mouse fixed on a board (1.0 mm thick) in the standing position under general anesthesia. Sequential images of the hind limb were obtained by the injection of non-ionic contrast material (1 ml/s for 2 s, Iopamidol, Nihon Schering, Tokyo, Japan) via the arterial catheter [*30*] on day 0 and day 14. Monochromatic synchrotron radiation with an energy level of 33.3 keV was obtained with a silicon crystal from beamlines NE5 and BL-14 at the High Energy Accelerator Research Organization, Tsukuba, Japan. To improve contrast resolution, subtraction images were created in the computer from the digital images obtained immediately before and during contrast material injection [*31*]. Angiogenesis was evaluated in terms of vessel density and assigned an angiographic score [*28, 32, 33*]. The ischemic signal in the acute phase is a critical factor inducing angiogenesis [*34*], and angiogenesis increases in proportion to the degree of ischemia [*35, 36*]. Therefore, angiogenesis should be compared among groups with comparable severity of acute ischemic injury. For this reason, we compared results among groups using only animals with grade I ischemic score (refer to Figure 3).

FITC gel angiography—To visualize microvessel networks, the FITC-gelatin conjugate fluorescence injection method (dialyzed FITC, 30 mg/mL conjugated gelatin solution) was employed [*37*]. Mice were anesthetized with pentobarbital sodium (50 mg/kg, i.p.), and a PE-10 (10-gauge polyethylene) catheter was placed in the right common carotid artery. The FITC gelatin solution (20 ml) was injected into the catheter

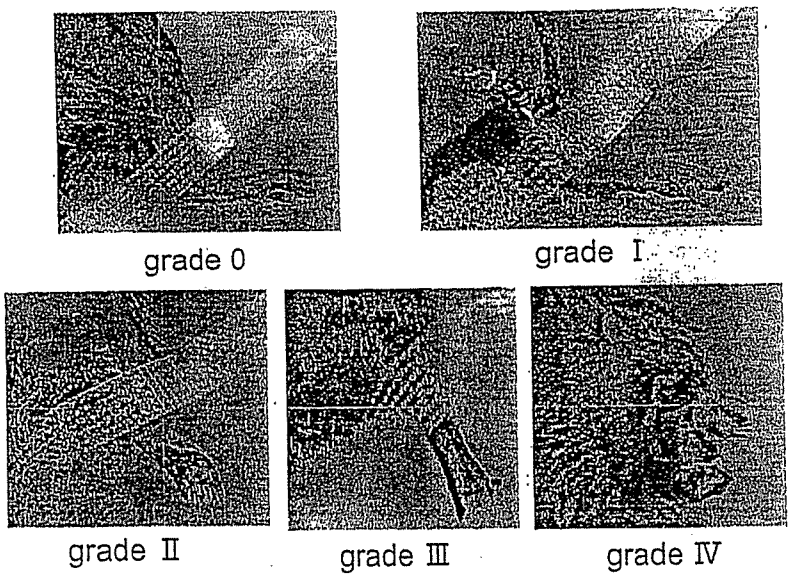

grade	necrotic area
0	none
I	only toes
II	extending to dorsum pedis
III	extending to crus
IV	extending to thigh or complete necrosis

Fig. 1. The grading of necrosis in ischemic hindlimb. The ischemic limb was macroscopically evaluated by using a graded morphological scale for tissue necrosis area (grade 0 to IV).

(1 ml/min) and the right common carotid vein was cut. After complete perfusion, the left leg were resected and immediately fixed in ice-cold graded paraformaldehyde (4%). A confocal laser scanning microscopy (CLSM) system (LSM-410, Carl Zeiss, Jena, Germany), equipped with a 488-nm argon laser (for FITC), was employed on thick sections (1–2 mm) to visualize microvessel networks in detail [*38*]. After computer-assisted 3-D imaging of microvessel networks by the CLSM system, the images were stored on hard disk memory or a magnetic optical disk, EDM-230C (Sony, Tokyo, Japan) and were printed with a digital Pictrostat 400 (Fuji Film Co/Ltd., Tokyo, Japan).

Statistical Analysis

Data are presented as mean values ± SD. Differences were assessed by using one-way ANOVA with Tukey's post test.

Results

Acute ischemic injury

Serum CK value—Firstly, we measured serum CK value to evaluate the acute ischemic injury in the three experimental groups. In the control (Wild) group, the serum CK value was 251 ± 34.7 IU/l. The serum CK values in the Wild + AG group (587.2 ± 128.7 IU/l) and iNOS-KO group (497 ± 126.7 IU/l) were significantly higher than that in the Wild group (Figure 2).

Ischemic score on day 7—The ischemic scores in the iNOS-KO group (92%) and the Wild + AG group (66.6%) were significantly higher than that in the Wild group (23%) (Figure 3). Percentages of grade I in the Wild, iNOS-KO and Wild + AG groups were 23%, 25% and 33%, respectively.

Chronic angiogenesis

Laser Doppler (non contact type) measurement—The

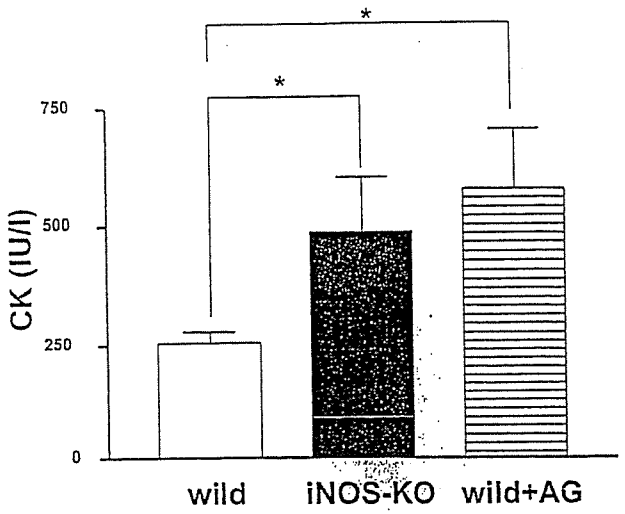

Fig. 2. Serum CK value in acute hindlimb ischemia. Open bar, control group; closed bar, iNOS-knockout (iNOS-KO) group; hatched bar, aminoguanidine-treated group (Wild + AG). The CK values in the iNOS-KO group and Wild + AG group were significantly higher than that in the control (Wild) group (*p<0.05).

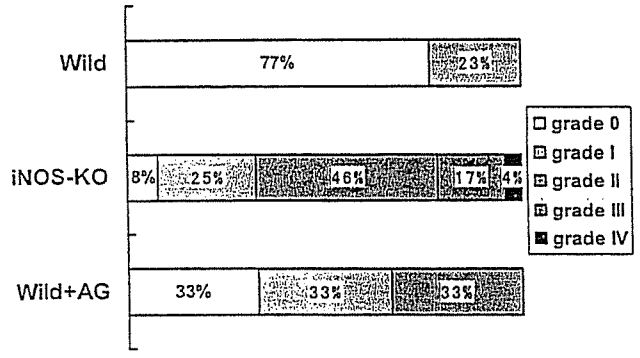

Fig. 3. Ischemic score in acute hindlimb ischemia. Open column, grade 0; dotted column, grade I; vertically lined column, grade II; hatched column, grade III; cross lined column, grade IV.

blood flow at the ischemic lesion was significantly reduced in all three groups on day 3 after surgery. However, at post-operative day 14, it was significantly higher in the iNOS-KO group (58.7 ± 8.7%) than in the Wild group (38.1 ± 5.2%) or the Wild + AG group (43.5 ± 6.4%) (Figure 4).

Sequential microangiography in in vivo—No vessels were apparent in hind limb angiography on day 0, and fine vessels were barely visible on day 14 in the Wild group (Figure 5 A and B). In contrast, many vessels were supplying the hind-limb on the injured side on day 14 in the iNOS-KO group. The angiogenic score on day 14 was significantly increased in the iNOS-KO group (0.29 ± 0.02) compared with that in

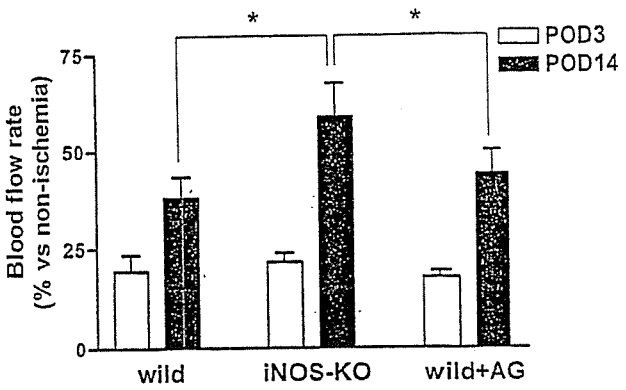

Fig. 4. Blood flow rate in non-contact laser-Doppler flowmetry. Open bar, blood flow ratio on day 3. Closed bar, blood flow ratio on day 14. The blood flow ratio on day 14 in the iNOS-KO group was significantly higher than in the Wild group or Wild + AG group (*p<0.05).

the Wild group or the Wild + AG group (0.12 ± 0.01 and 0.15 ± 0.02, respectively) (p<0.05) (Figure 5).

FITC angiography—The presence of fine vascular networks in the iNOS-KO group (Fig. 6B) implies that marked angiogenesis had occurred. There was a distinct difference in induction of vascular networks between the iNOS-KO group and the Wild and Wild + AG groups (Figure 6 A,B,C).

Discussion

In this experiment, ischemic injury was severe, but angiogenesis was markedly greater in the iNOS-KO group than in the Wild + AG or Wild group. The results indicate that NO generated by iNOS inhibited acute ischemic injury, but reduced angiogenesis in the chronic stage of ischemia.

Of the three NO synthese isoforms, nNOS is mainly localized in the central nervous system, postsynaptic density (PSD), and muscular sarcolemma (muscle fiber myelin) and participates in neural transmission [*39-41*]. iNOS is usually not expressed, but is induced in vascular smooth muscle cells and macrophages *via* cytokine stimulation during sepsis or ischemia with or without reperfusion, and produces large quantities of NO [*42*]. eNOS is mainly localized in vascular endothelial cells and produces NO continuously in response to shear stress, playing important roles in platelet aggregation and vasodilation [*12, 17*]. So, it appears reasonable that NO inhibits acute ischemic injury. In contrast, many studies have shown that NO production by iNOS aggravates injury in the hindlimb ischemia model. Nevertheless, we found that iNOS reduced ischemic injury in the acute stage in the present experiment. A key difference between our study and the others is the presence or absence of reperfusion following the ischemic period. We have

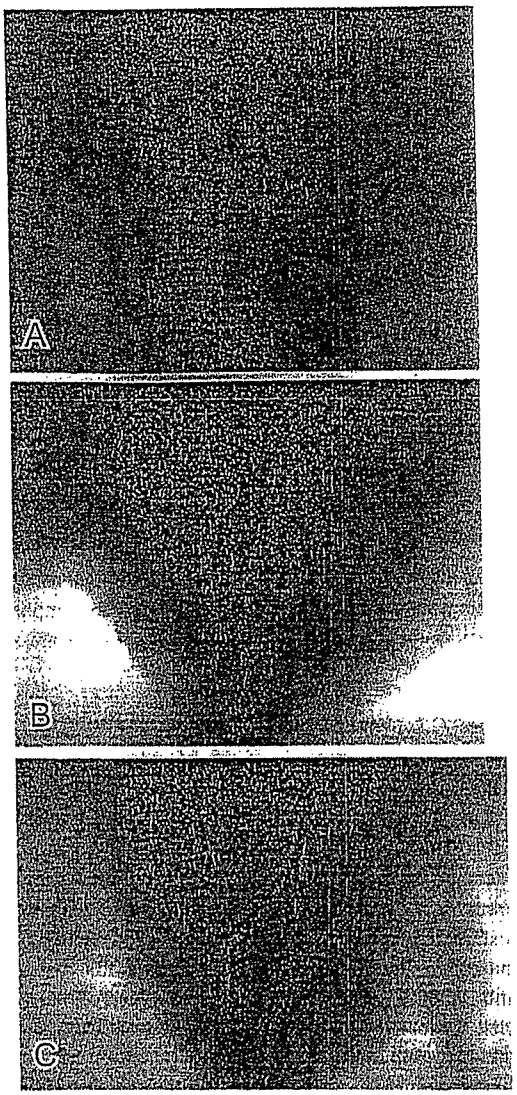

Fig. 5. Representative microangiograms. A : angiogram taken on day 0 in an animal of the Wild group ; B : angiogram taken on day 14 in an animal of the Wild group ; C : angiogram taken on day 14 in an animal of the iNOS-KO group.

already reported that superoxide ($O_2^{\cdot-}$) is produced in ischemic tissue at the time of reperfusion, and reacts with NO to form peroxynitrite [*43*]. Peroxynitrite is a potent oxidant that directly oxidizes sulfhydryl groups at a 1000-fold greater rate than hydrogen peroxide. It inhibits the function of various enzymes, including components of the mitochondrial electron transport chain. In our experiment, we examined ischemia without reperfusion, so that $O_2^{\cdot-}$ (and hence peroxynitrite) would not be produced, and only NO was present.

A second difference from previous experiments is that we used mice treated with iNOS inhibitor in the acute stage, as well as iNOS knockout mice, to examine the effect of iNOS [*44*]. It is noteworthy that one study in which iNOS knockout mice were used and reperfusion was not performed (similar to our protocol) found that injury was severe and angiogenesis in the chronic stage was augmented [*45*]. This is consistent with our results, and indicates that reperfusion plays a critical role in the outcome [*46*].

As the ischemic signal in the acute phase is a critical factor inducing angiogenesis [*34*], and angiogenesis increases in proportion to the degree of ischemia [*35, 36*], angiogenesis has to be compared among groups with comparable severity of acute ischemic injury. We therefore selected animals with grade I ischemic score in all cases for comparison among groups. Aminoguanidine was administered for only three days in the Wild + AG group in order to allow iNOS to function in the chronic stage. At corresponding levels of acute ischemia, angiogenesis in the chronic stage was obviously enhanced in the iNOS-KO group in comparison with the Wild + AG group, i.e., angiogenesis in the chronic stage was inhibited by the function of iNOS.

Many reports indicate that iNOS enhances angiogenesis in various neoplastic disease models [*44, 47–49*]. However, factors secreted by the cancer cells may play important roles in these models. It is important to note that our results showing a biphasic action of iNOS depended on the use of both an acutely iNOS inhibitor-treated wild-type group and an iNOS knockout group in an ischemic model. The mechanism underlying the inhibitory action of NO appears to be down-regulation of the VEGF receptor [*50*]. Possible compensatory roles of eNOS and nNOS in iNOS knockout mice have been ruled out by a previous study, in which their expression was shown to remain unchanged [*51*].

In summary, we have shown that iNOS reduces acute ischemia, but inhibits angiogenesis in a hindlimb ischemia model. Thus we suggest to use iNOS inducer or agents to increase NO production such as arginine with acute phase and supplement iNOS inhibitor in chronic stage. However these remained to be examined prior to clinical trial.

Acknowledgment

This work was supported by grants from Tokai University School of Medicine Research Aid in 2004, the research and study program of Tokai University Educational System General Research Organization and Kanagawa Nanbyou Foundation in 2004, as well as a Grant-in-Aid for Scientific Research in 2003 (No. 15659285) from the Ministry of Education, Science and Culture, Japan and Health and Labour Sciences Research Grants for Research on Human Genome, Tissue Engineering Food Biotechnology in 2003 (H15-saisei-003).

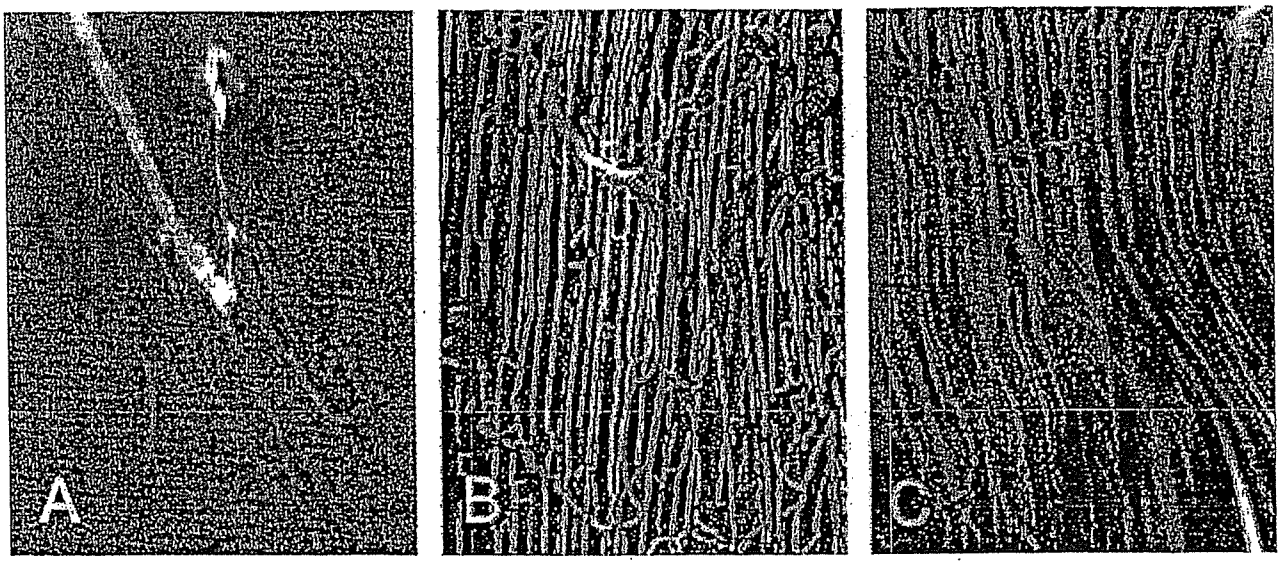

Fig. 6. FITC angiography. FITC angiograms were evaluated on day 14. A: in an animal of the Wild group; B: in an animal of the iNOS-KO group; C: in an animal of the Wild + AG group. Clear angiogenesis was visualized in the iNOS-KO group compared with the control group and aminoguanidine-treated group.

References

[1] Rosamond, W.D., Chambless, L.E., Folsom, A.R., Cooper, L.S., Conwill, D.E., Clegg, L., Wang, C.H., and Heiss, G.: Trends in the incidence of myocardial infarction and in mortality due to coronary heart disease, 1987 to 1994. *N. Engl. J. Med.*, 339, 861-867, 1998.

[2] Mukherjee, D., Bhatt, D.L., Roe, M.T., Patel, V., and Ellis, S.G.: Direct myocardial revascularization and angiogenesis-How many patients might be eligible? *Am. J. Cardiology.*, 84, 598-600, 1999.

[3] Isner, J.M. and Asahara, T.: Angiogenesis and vasculogenesis as therapeutic strategies for postnatal neovascularization. *J. Clin. Invest.*, 103, 1231-1236, 1999.

[4] Carmeliet, P., Ng, Y.S., Nuyens, D., Theilmeier, G., Brusselmans, K., Cornelissen, I., Ehler, E., Kakkar, V.V., Stalmans, I., Mattot, V., Perriard, J.C., Dewerchin, M., Flameng, W., Nagy, A., Lupu, F., Moons, L., Collen, D., Amore, P.A.D., and Shima, D.T.: Impaired myocardial angiogenesis and ischemic cardiomyopathy in mice lacking the vascular endothelial growth factor isoforms $VEGF_{164}$ and $VEGF_{188}$. *Nature. Med.*, 5, 495-502, 1999.

[5] Jayasnkar V., Woo J., Bish L.T., Pirolli T.J., Chatterjee S., Berry M.F., Burdick J., Gardner T.J., and Sweeney H.L.: Gene transfer of hepatocyte growth factor attenuates postinfarction heart failure. *Circulation*, 108[suppl II], II-230-II-236, 2003.

[6] Taniyama, Y., Morishita, R., Hiraoka, K., Aoki, M., Nakagami, H., Yamasaki, K., Matsumoto, K., Nakamura, T., Kaneda, Y., and Ogihara,T.: Therapeutic angiogenesis induced by human hepatocyte growth factor gene in rat diabetic hind limb ischemia model. Molecular mechanisms of delayed angiogenesis in diabetes. *Circulation*, 104, 2344-2350, 2001.

[7] Grines, C.L., Watkins, M.W., Helmer, G., Penny, W., Brinker, J., Marmur, J.D., West, A., Rade, J.J., Marrott, P., Hammond, H.K. and Engler, R.L.: Angiogenic gene therapy (AGENT) trial in patients with stable angina pectoris. *Circulation*, 105, 1291-1297, 2002.

[8] Tateishi-Yuyama, E., Matsubara, H., Murohara, T., Ikeda, U., Shintani, S., Masaki, H., Amano, K., Kishimoto, Y., Yoshimoto, K., Akashi, H., Shimada, K., Iwasaka, T., and Imaizumi, T.: Therapeutic angiogenesis for patients with limb ischemia by autologous transplantation of bone-marrow cells: a pilot study and a randomized controlled trial. *Lancet*, 360, 427-435, 2002.

[9] Randomski, M.W., Vallance, P., Whitley, G., Foxwell, N., and Moncada, S.: Platelet adhesion to human vascular endothelium is modulated by constitutive and cytokine induced nitric oxide. *Cardiovasc. Res.*, 27, 1380-1382, 1993.

[10] Förstermann, U., Closs, E.I., Pollock, J.S., Nakane, M., Schwarz, P., Gath, I., and Kleinert, H.: Nitric oxide synthase isozymes characterization, molecular cloning, and functions. *Hypertension*, 23, 1121-1131, 1994.

[11] Ziche, M., Morbidelli, L., Masini, E., Amerini, S., Granger, H.J., Maggi, C.A., Geppetti, P., and Ledda, F.: Nitric Oxide Mediates Angiogenesis *in vivo* and endothelial cell growth and migration *in vitro* promoted by substance P. *J. Clin. Invest.*, 94, 2036-2044, 1994.

[12] Papapetropoulos, A., Desai, K.M., Rudic, R.D., Mayer, B., Zhang, R., Ruiz-Torres, M.P., García-Cardeña, G., Madri, J.A., and Sessa, W.C.: Nitric oxide synthase inhibitors attenuate transforming-growth-factor-β_1-stimulated capillary organization *in vitro*. *Am. J. pathol.*, 150, 1835-1844, 1997.

[13] Ziche, M., Morbidelli, L., Choudhuri, R., Zhang, H.T., Donnini, S., Granger, H.J., and Bicknell, R.: Nitric oxide

synthase lies downstream from vascular endothelial growth factor-induced but not basic fibroblast growth factor-induced angiogenesis. *J. Clin. Invest.*, 99, 2625-2634, 1997.

[14] Papapetropoulos, A., García-Cardeña, G., Madri, J.A., and Sessa, W.C.: Nitric oxide production contributes to the angiogenic properties of vascular endothelial growth factor in human endothelial cells. *J. Clin. Invest.*, **100**, 3131-3139, 1997.

[15] Park, K.M., Byun, J.Y., Kramers, C., Kim, J.I., Huang, P.L., and Bonventre, J.V.: Inducible nitoric-oxide synthase is an important contributor to prolonged protective effects of ischemic preconditioning in the mouse kidney. *J. Biol. Chem.*, 278, 27256-27266, 2003.

[16] Murohara, T., Asahara, T., Silver, M., Bauters, C., Masuda, H., Kalka, C., Kearney, M., Chen, D., Symes, J.F., Fishman, M.C., Huang, P.L., and Isner, J.M.: Nitric oxide synthase modulates angiogenesis in response to tissue ischemia. *J. Clin. Invest.*, **101**, 2567-2578, 1998.

[17] Brevetti, L.S., Chang, D.S., Tang, G.L., Sarkar, R., and Messina, L.M.: Overexpression of endothelial nitric oxide synthase increases skeletal muscle blood flow and oxygenation in severe rat hind limb ischemia. *J. Vasc. Surg.*, 38, 820-826, 2003.

[18] Wildhirt, S.M., Suzuki, H., Horstman, D., Weismüller, S., Dudek, R.R., Akiyama, K., and Reichart, B.: Selective modulation of inducible nitric oxide synthase isozyme in myocardial infarction. *Circulation*, 96, 1616-1623, 1997.

[19] Misko, T.P., Moore, W.M., Kasten, T.P., Nickols, G.A., Corbett, J.A., Tilton, R.G., McDaniel, M.L., Williamson, J.R., and Currie, M.G.: Selective inhibition of the inducible nitric oxide synthase by aminoguanidine. *Eur. J. Pharmacol.*, 233, 119-125, 1993.

[20] Joly, G.A., Ayres, M., Chelly, F., and Kilboum, R.G.: Effects of NG-methyl-L-arginine, NG-nitro-L-arginine, and aminoguanidine on constitutive and inducible nitric oxide synthase in rat aorta. *Biochem. Biophys. Res. Commun.*, **199**, 147-154, 1994.

[21] Cross, A.H., Misko T.P., Lin, R.F., Hickey, W.F., Trotter, J.L., and Tilton, R.G.: Aminoguanidine, an inhibitor of inducible nitric oxide synthase, ameliorates experimental autoimmune encephalomyelitis in SJL mice. *J. Clin. Invest.*, **93**, 2684-2690, 1994.

[22] Niu, X.L., Yang, X., Hoshiai, K., Tanaka, K., Swamura, S., Koga, Y., and Nakazawa, H.: Inducible nitric oxide synthase deficiency dose not affect the susceptibility of mice to atherosclerosis but increases collagen content in lesions. *Circulation*, 103, 1115-1120, 2001.

[23] Wolff, D.J., Gauld, D.S., Neulander, M.J., and Southan, G.: Inactivation of nitric oxide synthase by substituted aminoguanidines and aminoisothioureas. *J. Pharmacol. Exp. Ther.*, 283, 265-273, 1997.

[24] Wildhirt, S.M., Schulze, C., Conrad, N., Kornberg, A., Horstman, D., and Reichart, B.: Aminoguanidine inhibits inducible NOS and reverses cardiac dysfunction late after ischemia and reperfusion-implications for iNOS-mediated myocardial stunning. *Thorac. Cardiovasc. Surg.*, 47, 137-143, 1999.

[25] Tamarat, R., Silvestre, J.S., Huijberts, M., Benessiano, J., Ebrahimian, T.G., Duriez, M., Wautier, M.P., Wautier, J.L., and Lévy, B.I.: Blockade of advanced glycation end-product formation restores ischemia-induced angiogenesis in diabetic mice. *Proc. Natl. Acad. Sci. U. S. A.*, **100**, 8555-8560, 2003.

[26] Couffinhal, T., Silver, M., Zheng, L.P., Kearney, M., Witzenbichler, B., and Isner, J.M.: Mouse model of angiogenesis. *Am. J. Pathol.*, 152, 1667-1679, 1998.

[27] Kasahara, H., Tanaka, E., Fukuyama, N., Sato, E., Sakamoto, H., Tabata, Y., Ando, K., Iseki, H., Shinozaki, Y., Kimura, K., Kuwabara, E., Koide, S., Nakazawa, H., and Mori, H.: Biodegradable gelatin hydrogel potentiates the angiogenic effect of fibroblast growth factor 4 plasmid in rabbit hindlimb ischemia. *J. Am. Coll. Cardiol.*, 41, 1056-1062, 2003.

[28] Tanaka, E., Hattan, N., Ando, K., Ueno, H., Sugio, Y., Mohammed, M.U., Voltchikhina, S.A., and Mori H.: Amelioration of microvascular myocardial ischemia by gene transfer of vascular endothelial growth factor in rabbits. *J. Thorac. Cardiovasc. Surg.*, **120**, 720-728, 2000.

[29] Lindén, M., Sirsjö, A., Lindbom, L., Nilsson, G., and Gidlöf, A.: Laser-Doppler perfusion imaging of microvascular blood flow in rabbit tenuissimus muscle. *Am. J. Physiol. Heart Circ. Physiol.*, **269**, H1496-H1500, 1995.

[30] Kuwabara, E., Furuyama, F., Ito, K., Tanaka, E., Hattan, N., Fujikura, H., Kimura, K., Goto, T., Hayashi, T., Taira, H., Shinozaki, Y., Umetani, K., Hyodo, K., Tanioka, K., Mochizuki, R., Kawai, T., Koide, S., and Mori, H.: Inhomogeneous vasodilatory responses of rat tail arteries to heat stress: evaluation by synchrotron radiation microangiography. *Jpn. J. Physiol.*, 52, 403-408, 2002.

[31] Sekka, T., Volchikhina, S.A., Tanaka, A., Hasegawa, M., Tanaka, Y., Ohtani, Y., Tajima, T., Makuuchi, H., Tanaka, E., Iwata, Y., Sato, S., Hyodo, K., Ando, M., Umetani, K., Kubota, M., Tanioka, K., and Mori, H.: Visualization, quantification and therapeutic evaluation of angiogenic vessels in cancer by synchrotron microangiography. *J. Synchrotron Rad.*, 7, 361-367, 2000.

[32] Takeshita, S., Zheng, L.P., Brogi, E., Kearney, M., Pu, L.G., Bunting, S., Ferrara, N., Symes, J.F., and Isner, J.M.: Therapeutic angiogenesis: a single intra-arterial bolus of vascular endothelial growth factor augments revascularization in a rabbit ischemic hind limb model. *J. Clin. Invest.*, 93, 662-670, 1994.

[33] Takeshita, S., Isshiki, T., Ochiai, M., Eto, K., Mori, H., Tanaka, E., Umetani, K. and Sato, T.: Endothelium-dependent relaxation of collateral microvessels after intramuscular gene transfer of vascular endothelial growth factor in a rat model of hindlimb ischemia. *Circulation*, 98, 1261-1263, 1998.

[34] Chung, N.A.Y., Lydakis, C., Belgore, F., Blann, A.D., and Lip, G.Y.H.: Angiogenesis in myocardial infarction An acute or chronic process? *Eur. Heart J.*, 23, 1604-1608, 2002.

[35] Gavin, J.B., Maxwell, L., and Edgar, S.G.: Microvascular Involvement in Cardiac Pathology. *J. Mol. Cell. Cardiol.*, 30, 2531-2540, 1998.

[36] Sennlaub, F., Courtois, Y., and Goureau, O. Inducible nitric

oxide synthase mediates the change from retinal to vitreal neovascularization in ischemic retinopathy. *J. Clin. Invest.*, 107, 717-725 2001.

[37] Itoh, J., Kawai, K., Serizawa, A., Yasumura, K., Ogawa, K., and Osamura, R.Y.: A new approach to three-dimensional reconstructed imaging of hormone-secreting cells and their microvessel environments in rat pituitary glands by confocal laser scanning microscopy. *J. Histochem. Cytochem.*, 48, 569-577, 2000.

[38] Itoh, J., Yasumasa, K., Takeshita, T., Ishikawa, H., Kobayashi, H., Ogawa, K., Kawai, K., Serizawa, A., and Osamura, R.Y.: Three-dimensional imaging of tumor angiogenesis. *Analyt. Quant. Cytol. Histol.*, 22, 85-90, 2000.

[39] Kobzik, L., Reid, M.B., Bredt, D.S., and Stamler, J.S.: Nitric oxide in skeletal muscle. *Nature*, 372, 546-548 1994.

[40] Brenman, J.E., Christopherson, K.S., Craven, S.E., McGee, A.W., and Bredt, D.S.: Cloning and Characterization of Postsynaptic Density 93, a Nitric Oxide Synthase Interacting Protein. *J. Neurosci.*, 16, 7407-7415, 1996.

[41] Dreyer, J., Schleicher, M., Tappe, A., Schilling, K., Kuner, T., Kusumawidijaja, G., Müller-Esterl, W., Oess, S., and Kuner, R.: Nitric Oxide Synthase (NOS)-Interacting Protein Interacts with Neuronal NOS and Regulates Its Distribution and Activity. *J. Neurosci.*, 24, 10454-10465, 2004.

[42] Sharshar, T., Gray, F., Geoffroy, L.G., Hopkinson, N.S., Ross, E., Dorandeu, A., Orlikowski, D., Raphael, J.C., Gajdos, P., and Annane, D.: Apoptosis of neurons in cardiovascular autonomic centres triggered by inducible nitric oxide synthase after death from septic shock. *Lancet*, 362, 1799-1805 2003.

[43] Liang, F., Gao, E., Tao, L., Liu, H., Ou, Y., Christopher, T.A., Lopez, B.L., and Ma, X.L.: Critical timing of L-arginine treatment in post-ischemic myocardial apoptosis—role of NOS isoforms. *Cardiovasc. Res.*, 62, 568-577, 2004.

[44] Kane, A.J., Barker, J.E., Mitchell, G.M., Theile, D.R.B., Romero, R., Messina, A., Wagh, M., Fraulin, F.O.G., Morrison, W.A., and Stewart, A.G.: Inducible nitric oxide synthase (iNOS) activity promotes ischemic skin flap survival. *Br. J. Pharmacol.*, 132, 1631-1638, 2001.

[45] Cuzzocrea, S., Chatterjee, P.K., Mazzon, E., Dugo, L., De Sarro, A., Van de Loo, F.A., Caputi, A.P., and Thiemermann, C.: Role of induced nitric oxide in the initiation of the inflammatory response after postischemic injury. *Shock*, 18, 169-176, 2002.

[46] Bolli, R.: Cardioprotective function of inducible nitric oxide synthase and role of nitric oxide in myocardial ischemia and preconditioning: an overview of a decade of research. *J. Mol. Cell. Cardiol.*, 33, 1897-918, 2001.

[47] Kisley, L.R., Barrett, B.S., Bauer, A.K., Dwyer-Nield, L.D., Barthel, B., Meyer, A.M., Thompson, D.C., and Malkinson, A.M.: Genetic ablation of inducible nitric oxide synthase decreases mouse lung Tumorigenesis. *Cancer. Res.*, 62, 6850-6856 2002.

[48] Deininger, M.H., Wybranietz, W.A., Graepler, F.T., Lauer, U.M., Meyermann, R., and Schluesener, H.J.: Endothelial endostatin release is induced by general cell stress and modulated by the nitric oxide/cGMP pathway. *F.A.S.E.B. J.*, 17, 1267-1276 2003.

[49] Cianchi, F., Cortesini, C., Fantappiè, O., Messerini, L., Sardi, I., Lasagna, N., Perna, F., Fabbroni, V., Felice, A.D., Perigli, G., Mazzanti, R., and Masini, E.: Cyclooxygenase-2 activation mediates the proangiogenic effect of nitric oxide in colorectal cancer. *Clin. Cancer. Res.*, 10, 2694-2704, 2004.

[50] Fukumura, D., Gohongi, T., Kadambi, A., Izumi, Y., Ang, J., Yun, C.O., Buerk, D.G., Huang, P.L., and Jain, R.K.: Predominant role of endothelial nitric oxide synthase in vascular endothelial growth factor-induced angiogenesis and vascular permeability. *Proc. Natl. Acad. Sci. U. S. A.*, 98, 2604-2609, 2001.

[51] Qi, W., Chen, L.E., Zhang, L., Eu, J.P., Seaber, A.V., and Urbaniak, J.R.: Reperfusion injury in skeletal muscle is reduced in inducible nitric oxide synthase knockout mice. *J. Appl. Physiol.*, 97, 1323-1328, 2004.

Available online at www.sciencedirect.com
ScienceDirect
Neurochemistry International 49 (2006) 448–453
NEUROCHEMISTRY International
www.elsevier.com/locate/neuint

Effect of sustained limb ischemia on norepinephrine release from skeletal muscle sympathetic nerve endings

Yosuke Kuroko [a], Noriyuki Tokunaga [b], Toji Yamazaki [b,*], Tsuyoshi Akiyama [b], Kozo Ishino [a], Shunji Sano [a], Hidezo Mori [b]

[a] *Department of Cardiovascular Surgery, Okayama University Graduate School of Medicine and Dentistry, Okayama 700-8558, Japan*
[b] *Department of Cardiac Physiology, National Cardiovascular Center Research Institute, 5-7-1 Fujishiro-dai, Suita, Osaka 565-8565, Japan*

Received 8 October 2005; accepted 2 March 2006
Available online 24 April 2006

Abstract

Acute ischemia has been reported to impair sympathetic outflow distal to the ischemic area in various organs, whereas relatively little is known about this phenomenon in skeletal muscle. We examined how acute ischemia affects norepinephrine (NE) release at skeletal muscle sympathetic nerve endings. We implanted a dialysis probe into the adductor muscle in anesthetized rabbits and measured dialysate NE levels as an index of skeletal muscle interstitial NE levels. Regional ischemia was introduced by microsphere injection and ligation of the common iliac artery. The time courses of dialysate NE levels were examined during prolonged ischemia. Ischemia induced a decrease in the dialysate NE level (from 19 ± 4 to 2.0 ± 0 pg/ml, mean ± S.E.), and then a progressive increase in the dialysate NE level. The increment in the dialysate NE level was examined with local administration of desipramine (DMI, a membrane NE transport inhibitor), ω-conotoxin GVIA (CTX, an N-type Ca^{2+} channel blocker), or TMB-8 (an intracellular Ca^{2+} antagonist). At 4 h ischemia, the increment in the dialysate NE level (vehicle group, 143 ± 30 pg/ml) was suppressed by TMB-8 (25 ± 5 pg/ml) but not by DMI (128 ± 10 pg/ml) or CTX (122 ± 18 pg/ml). At 6 h ischemia, the increment in the dialysate NE level was not suppressed by the pretreatment. Ischemia induced biphasic responses in the skeletal muscle. Initial reduction of NE release may be mediated by an impairment of axonal conduction and/or NE release function, while in the later phase, the skeletal muscle ischemia-induced NE release was partly attributable to exocytosis via intracellular Ca^{2+} overload rather than opening of calcium channels or carrier mediated outward transport of NE.
© 2006 Elsevier Ltd. All rights reserved.

Keywords: Catecholamine; Interstitial space; Microdialysis; Rabbit; Striate muscle

1. Introduction

Acute ischemia has been reported to be associated with impairment of the sympathetic tract (Schömig et al., 1984; Toyohara et al., 1986; Fujii et al., 2003). A well-known example is myocardial ischemia associated with impairment of the regional cardiac sympathetic nerve endings (Schömig et al., 1984; Ciuffo et al., 1985). Outward norepinephrine (NE) transport through uptake$_1$ carrier has been proposed as one of the main mechanisms responsible for ischemia-induced NE efflux from sympathetic nerve endings (Schömig et al., 1984; Akiyama and Yamazaki, 2001). However, little is known about the sympathetic impairment evoked by skeletal muscle ischemia. Histochemical and electrophysiological studies (Barker and Saito, 1981; Hill et al., 1996) have identified sympathetic innervation in skeletal muscle, which exerted actions on the regulation of regional blood flow and glucose metabolism (Thompson and Mohrman, 1983; Fagius and Berne, 1994). During and after exercise, muscle sympathetic nerve activity has been reported to be modulated by ischemia-induced metaboreceptor stimulation (Cornett et al., 2000; Cui et al., 2001). Furthermore, skeletal muscle may be exposed to prolonged severe ischemia (Welsh and Lindinger, 1993). Severe skeletal muscle ischemia occurs with trauma, vascular diseases, and compartment syndrome. It is so far unknown whether severe muscle ischemia induces excessive NE release from muscle sympathetic nerve endings.

In view of energy metabolism, cardiac ischemia is characterized by rapid deterioration of cardiac function, which has been linked to a fall in intracellular pH, increased levels of inorganic phosphate and reduction in free energy changes of ATP-hydrolysis (Mair, 1999). In contrast to cardiac muscle,

* Corresponding author. Tel.: +81 6 6833 5012; fax: +81 6 6872 8092.
E-mail address: yamazaki@ri.ncvc.go.jp (T. Yamazaki).

0197-0186/$ – see front matter © 2006 Elsevier Ltd. All rights reserved.
doi:10.1016/j.neuint.2006.03.004

energy requirements in skeletal muscle are dependent on exercise and are reduced in the resting state since only resting tone is maintained (Idström et al., 1990; Lindsay et al., 1990). Typically, prolonged skeletal muscle ischemia imposes a metabolic stress that results in a depletion of glycogen, high-energy phosphagen, and adenine nucleotides (Welsh and Lindinger, 1993). Thus, a differential time course of energy metabolism occurs in the skeletal muscle and cardiac myocardium. No studies have systematically characterized the impairment of sympathetic nerves in the skeletal muscle ischemia.

Recently, we reported that microdialysis technique with high-performance liquid chromatography is a sensitive and versatile method for monitoring interstitial NE concentrations in myocardial ischemic regions (Akiyama et al., 1991, 1993). Moreover, we applied microdialysis technique to skeletal muscle and have reported that skeletal muscle dialysate NE serves as an index of muscle sympathetic nerve activity (Tokunaga et al., 2003a). Using this method, we investigated how acute skeletal muscle ischemia affects NE release from skeletal muscle sympathetic nerve endings and the mechanism of skeletal muscle ischemia-induced NE release with regional pharmacological intervention.

2. Methods

2.1. Animal model

The investigation conformed with the *Guide for the Care and Use of Laboratory Animals* published by the US National Institutes of Health (NIH Publication No. 85-23, revised 1996). Forty-two male Japanese white rabbits weighing 2.2–3.8 kg were used for the model of skeletal muscle ischemia. The animals were anesthetized with pentobarbital sodium (30–35 mg/kg) and ventilated with room air mixed with oxygen. The level of anesthesia was maintained with a continuous intravenous infusion of pentobarbital sodium (1–2 mg/kg/h). Body temperature was maintained with a heated pad and lamp. An electrocardiogram, heart rate (HR), and mean arterial blood pressure (MAP) were simultaneously monitored with a data recorder. After a longitudinal skin incision was made in the left groin, the dialysis probes were implanted in the left adductor muscle with a fine guiding needle.

2.2. Dialysis technique and NE measurements

With the dialysis technique, dialysate NE levels were measured as an index of skeletal muscle interstitial NE levels. For skeletal muscle dialysis, we designed a transverse dialysis probe. The dialysis fiber (13 mm length, 0.31 mm o.d. and 0.2 mm i.d.; PAN-1200, 50,000 molecular mass cut-off, Asahi Chemical, Tokyo, Japan) was glued at both ends into a polyethylene tube (25 cm length, 0.5 mm o.d. and 0.2 mm i.d.) (Akiyama et al., 1991). The dialysis probe was perfused with Ringer solution using a microinjection pump (CMA 102, Carnegie Medicin, Stockholm, Sweden). Similar to previous studies (Tokunaga et al., 2003a, 2003b), we chose a perfusion speed of 10 μl/min for skeletal muscle. Sampling periods were set at 15 min for skeletal muscle. Dialysate NE levels were measured by high-performance liquid chromatography with electrochemical detection (ECD-300, Eicom, Kyoto, Japan) after removing interfering compounds in the dialysate by an alumina procedure (Anton and Sayer, 1962; Akiyama et al., 1991). Dialysate dihydroxyphenylglycol (DHPG) levels were measured by separate high-performance liquid chromatography with electrochemical detection (Akiyama and Yamazaki, 2001).

2.3. Experimental protocols

Acute skeletal muscle ischemia was induced by injection of non-radioactive iodine-labeled microspheres (15 μm in diameter, 3×10^7/kg, Sekisui Plastic, Osaka, Japan) through the left common iliac artery, as previously described (Tanaka et al., 2000). After the injection of microspheres, the common iliac artery was ligated.

2.3.1. Protocol 1: time courses of dialysate NE levels during acute ischemia

To examine the time courses of dialysate NE levels during acute skeletal muscle ischemia, we measured dialysate NE levels over 60-min periods of skeletal muscle ischemia ($n = 6$). We collected four consecutive 15-min dialysate samples. Furthermore, we measured dialysate NE samples over a period of 6 h of skeletal muscle ischemia with 2 h interval in separate rabbits. To examine intraneuronal NE kinetics in the skeletal muscle, the measurement of dialysate DHPG level was added during 6 h of skeletal muscle ischemia ($n = 6$).

2.3.2. Protocol 2: involvement of NE uptake$_1$ transport, Ca^{2+} channels and cytosol Ca^{2+} in dialysate NE levels during acute ischemia

To examine the mechanism underlying the increment of NE release during the prolonged ischemia, dialysate NE levels were measured with regional pharmacological intervention. Neurotransmitter release from sympathetic nerve endings can be caused by a variety of different mechanisms (Schömig et al., 1987; Kawada et al., 2000; Akiyama and Yamazaki, 2001). In the present studies, we examined the roles of membrane NE transport, N-type Ca^{2+} channels and cytosol Ca^{2+} in the time courses of dialysate NE levels during prolonged ischemia. To examine the involvement of membrane NE transport in the ischemia-induced NE release, we locally administered an uptake$_1$ carrier blocker, desipramine (100 μM) through a dialysis probe and observed the responses of dialysate NE (Akiyama and Yamazaki, 2001) ($n = 6$). The same protocol was performed with addition of a voltage-dependent N-type Ca^{2+} channel blocker, ω-conotoxin GVIA (10 μM) ($n = 6$) or intracellular Ca^{2+} antagonist, 8-(*N*,*N*-diethylamino)-octyl-3,4,5-trimethoxybenzoate hydrochloride (TMB-8, 1 mM) ($n = 6$) through a dialysis probe. From data on protocol 1, we observed increases in dialysate NE levels after 2 h of skeletal muscle ischemia. Therefore, the time course of dialysate NE for skeletal muscle ischemia was examined over a period of 6 h with a 2 h-interval ($n = 6$). The effectiveness of ω-conotoxin GVIA (10 μM) ($n = 6$) or TMB-8 (1 mM) ($n = 6$) was tested before the experiment in separate rabbits. We administered high potassium (KCl, 100 mM) locally through the dialysis probe, and the dialysate NE response was obtained in the presence and absence of ω-conotoxin GVIA or TMB-8. High-K increased dialysate NE from 11.7 ± 2.8 to 84.7 ± 20.8 pg/ml ($n = 6$). This KCl-induced increment in dialysate NE was attenuated by the addition of ω-conotoxin GVIA or TMB-8 (Fig. 1).

2.3.3. Protocol 3: time courses of dialysate lactate levels during the hind limb ischemia

To confirm whether this perturbation induces tissue ischemia, we examined the time course of dialysate lactate levels as an index of tissue ischemia. The dialysate lactate levels were measured by kinetic enzymatic analysis with CMA 600 (Carnegie Medicin). In the skeletal muscle ischemia, four consecutive 15-

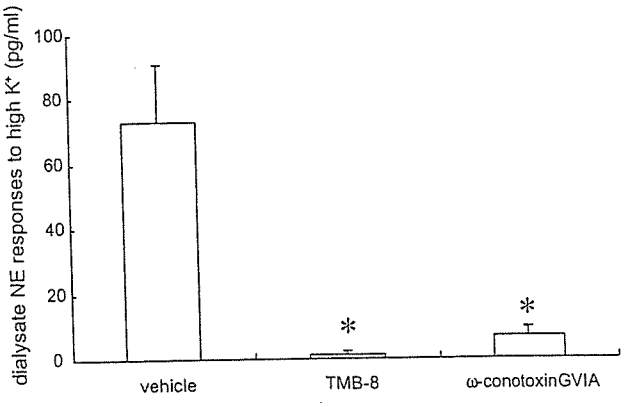

Fig. 1. Effects of pharmacological intervention on dialysate norepinephrine (NE) responses to high K^+ (KCl, 100 mM). Both TMB-8 (1 mM) and ω-conotoxin (10 μM) suppressed dialysate responses to high K^+. Values are means ± S.E. ($n = 6$).

min dialysate samples were collected during the initial 60-min and subsequently three consecutive samples were collected over a period of 6 h with a 2 h-interval ($n = 6$).

2.4. Statistical analysis

All data are presented as mean ± S.E. values. Hemodynamic and dialysate data responses to acute ischemia were statistically analyzed by analysis of variance with repeated measures. When a statistically significant effect of ischemia was detected as a whole, the Dunnett's test was applied to determine which mean values differed significantly from the control level. When a statistically significant effect of the treatment was detected, Newman–Keuls test was applied to determine which treatment differed significantly from the vehicle.

3. Results

Table 1 summarizes changes in HR and MAP. MAP and HR increased during 6 h-hind limb ischemia. Changes in MAP at 2 h and HR at 6 h-hind limb ischemia were significant.

3.1. Time courses of dialysate NE levels during short and prolonged ischemia

Skeletal muscle dialysate NE levels decreased from 19 ± 4 pg/ml at control to 9 ± 4 pg/ml at 30 min of ischemia and reached 2 ± 0 pg/ml at 60 min of ischemia (Fig. 2). The decrease in dialysate NE level was maintained after 2 h of ischemia. Then skeletal muscle dialysate NE levels markedly increased to 143 ± 30 pg/ml at 4 h of ischemia. The dialysate NE levels continued to increase progressively and reached 289 ± 45 pg/ml at 6 h of ischemia. Skeletal muscle dialysate DHPG levels decreased from 38 ± 2 pg/ml at control to 5 ± 1 pg/ml at 2 h of ischemia and reached 7 ± 1 pg/ml at 6 h of ischemia.

3.2. Involvement of NE uptake$_1$ transport, Ca^{2+} channels and cytosol Ca^{2+} in dialysate NE levels during prolonged ischemia

Dialysate NE increases at 4 and 6 h-skeletal muscle ischemia were not suppressed by treatment with desipramine (Fig. 3). Dialysate NE increases at 4 and 6 h-skeletal muscle ischemia were not suppressed by treatment with ω-conotoxin GVIA. Treatment with TMB-8 significantly suppressed the dialysate NE increase at 4 h-skeletal muscle ischemia. But at 6 h-skeletal muscle ischemia, there was no significant difference in dialysate NE levels among treatments.

Table 1
Changes in heart rate (HR) and mean arterial pressure (MAP) in 6 h-hindlimb ischemia

	Control	2 h	4 h	6 h
HR (beats/min)	283 ± 10	292 ± 4	293 ± 8	302 ± 8*
MAP (mmHg)	104 ± 6	114 ± 3*	111 ± 4	108 ± 4

Values are means ± S.E. from six rabbits. Data were obtained during control, after 2, 4, and 6 h of hind limb ischemia.
* $P < 0.05$ vs. control.

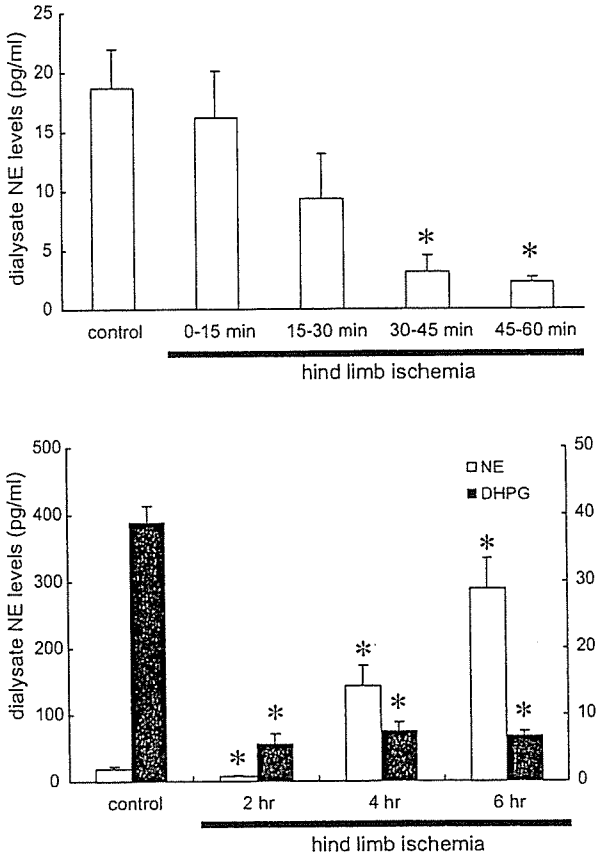

Fig. 2. (Upper panel) Time course of dialysate norepinephrine (NE) levels during 60 min-hind limb ischemia. Values are means ± S.E. ($n = 6$). *$P < 0.05$ vs. control value. (Lower panel) Time courses of dialysate NE and dihydroxyphenylglycol (DHPG) levels during 6 h-hind limb ischemia. Values are means ± S.E. ($n = 6$). *$P < 0.05$ vs. control value.

3.3. Time course of dialysate lactate levels during hind limb ischemia

Skeletal muscle dialysate lactate levels increased from 0.6 ± 0.07 nmol/l at control to 1.73 ± 0.17 nmol/l at 45–60 min

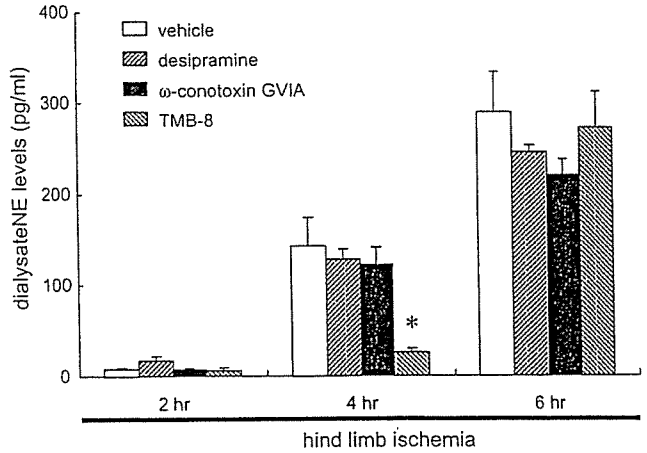

Fig. 3. Effects of pharmacological intervention on dialysate norepinephrine (NE) levels evoked by 6 h-hind limb ischemia. Desipramine (100 μM), ω-conotoxin (10 μM), or TMB-8 (1mM) was locally administered through the probe. Values are means ± S.E. ($n = 6$). *$P < 0.05$ vs. concurrent value of vehicle group.

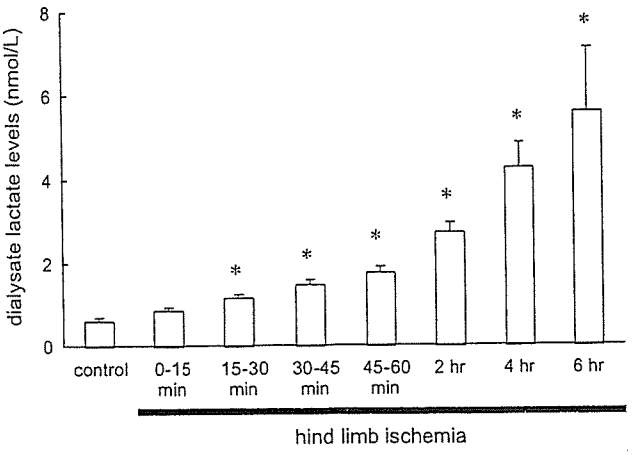

Fig. 4. Time course of dialysate lactate levels during 6 h-hind limb ischemia. Values are means ± S.E. ($n = 6$). $^*P < 0.05$ vs. control value.

of ischemia (Fig. 4). These step-wise increases were continued for 6 h of the hind limb ischemia.

4. Discussion

Using dialysis techniques in the in vivo rabbit skeletal muscle, we examined interstitial levels of NE in the control and ischemic period, and observed the biphasic response of dialysate NE in ischemic skeletal muscle. Ischemia induced an initial reduction followed by a progressive increment in dialysate NE levels. Here we discuss changes in interstitial NE and possible mechanisms underlying sympathetic nerve impairment.

Within 2 h of acute skeletal muscle ischemia, unlike acute myocardial ischemia, skeletal muscle interstitial NE levels continued to decline progressively, decreasing to one-tenth of control at 60 min of ischemia. A previous study demonstrated that skeletal muscle ischemia modulated the baroreflex control of regional muscle sympathetic activity (Cornett et al., 2000). At 75 min of acute skeletal muscle ischemia, hemodynamic responses to carotid occlusion were preserved while the interstitial NE response to carotid occlusion was blunted in the ischemic region (Tokunaga et al., 2003b). These results indicate that the systemic response to baroreflex remained intact while the skeletal muscle sympathetic response was impaired in ischemic regions. Earlier studies reported that acute limb ischemia reduced the conduction of motor nerves such as sciatic nerve (Fern and Harrison, 1994), and induced axonal degeneration histologically (Makitie and Teravainen, 1977; Nukada and Dyek, 1987). Axonal conduction in the ischemic muscle sympathetic nerve may be impaired as well as in sensory and motor nerves. In addition to diminished axonal conductance, the interstitial NE response to high K^+ but not tyramine was suppressed during the 75 min of acute skeletal muscle ischemia, although NE content at muscle sympathetic nerve endings was preserved during the ischemia (Tokunaga et al., 2003b). This result indicates that exocytotic NE releasing function in muscle sympathetic nerve endings might be suppressed during 75 min of acute skeletal muscle ischemia. Therefore, initial reduction of NE release may be mediated by an impairment of axonal conduction and/or NE releasing function.

After 2 h of acute skeletal muscle ischemia, skeletal muscle interstitial NE levels significantly increased and finally reached 20-fold that of control. This amount of NE release is higher than that evoked by baroreflex or high K^+. This level is similar to that evoked by the Na^+–K^+ ATPase inhibitor, ouabain (Tokunaga et al., 2003a). The amount of NE release evoked by ischemia may be dependent on the density of sympathetic innervation. Dispersed organ systems such as skeletal muscle have a thin and diffuse sympathetic innervation. This is the first report to describe that marked NE release is induced from muscle sympathetic nerve endings in the ischemic region after 2 h of skeletal muscle ischemia. Numerous histological changes of skeletal muscle have been reported after ischemia and reperfusion injury (Patterson and Klenerman, 1979; Turchányi et al., 2005). However, there is no histochemical evidence of the impaired sympathetic nerves in the skeletal muscle ischemia.

In the case of skeletal muscle ischemia, ω-conotoxin GVIA did not suppress NE efflux. N-type Ca^{2+} channels are not involved in this NE efflux. Desipramine did not alter NE efflux during skeletal muscle ischemia. Desipramine inhibits carrier-mediated NE transport in both directions. Considering that desipramine did not alter interstitial NE levels, the amounts of NE release and uptake via normal transport can be surmised to be negligible. Second, the increase in skeletal muscle interstitial NE levels was not associated with an increase in skeletal muscle interstitial DHPG levels, indicating that skeletal ischemia fails to induce axoplasmic NE elevation via alterations in monoamine activity, NE mobilization from stored vesicle, and NE uptake. Further, desipramine did not suppress NE efflux. These results exclude the possibility that marked increases in skeletal muscle interstitial NE could be due to carrier-mediated outward transport of NE for removal of elevated axoplasmic NE concentration. The membrane NE transporter exists in the skeletal muscle sympathetic nerve endings (Cabassi et al., 2001; Tokunaga et al., 2003a), but was not involved in outward transport of NE. Thus, we consider that a ω-conotoxin GVIA insensitive and desipramine-resistant NE release mechanism exists after 2 h of acute skeletal muscle ischemia.

TMB-8 significantly suppressed the marked NE release at 4 h of skeletal muscle ischemia. TMB-8 is well known to inhibit Ca^{2+} release from intracellular Ca^{2+} stores. TMB-8 inhibits caffeine-induced catecholamine release from perfused adrenal gland in the absence of extracellular Ca^{2+} (Yamada et al., 1988). Studies using chromaffin cells, brain slices and synaptosomes have suggested that metabolic inhibition induces intracellular Ca^{2+} overload (Milusheva et al., 1992), and a rise in the intracellular Ca^{2+} causes exocytotic catecholamine release without membrane depolarization (Dry et al., 1991; Du et al., 1997). Moreover, an in vitro study with adrenergic nerves of guinea-pig vas deferens suggested that Ca^{2+} release from intracellular Ca^{2+} stores is to some extent involved in the NE release evoked by elevation of intracellular Na^+ (Katsuragi et al., 1994). Under energy-depleted conditions, Ca^{2+} overload

in synaptosomes of noradrenergic neurons from the brain is an important mechanism for the enhanced release of neurotransmitter, with a reversal of Na^+–Ca^{2+} exchange possibly the key pathway leading to intraneuronal Ca^{2+} overload (Du et al., 1997). We consider that Ca^{2+} release from intracellular Ca^{2+} stores is partly involved in the NE release at 4 h of skeletal muscle ischemia.

At 6 h of skeletal ischemia, increment in dialysate NE level was not suppressed by the pretreatments. This result suggests that another mechanism may be involved in NE release, which is insensitive to desipramine, ω-conotoxin GVIA, and TMB-8. Alternatively, the NE release may occur with development of irreversible membrane damage and can no longer be inhibited by pharmacological interventions. Future work should concentrate on these aspects of NE release during the later period.

4.1. Methodological considerations

The limitation of this experiment is related to the methodology and the duration of the hind limb ischemia. In a variety of these experimental models for organ ischemia, we chose microsphere injection and iliac artery occlusion for the short and prolonged hind limb ischemia model. A preliminary experiment indicated that common iliac artery occlusion did not yield severe ischemia or muscle necrosis in a chronic ischemic model because collateral flow prevents skeletal muscle ischemia. The combination of artery occlusion and injection of microsphere was used for the hind limb ischemic model. In the hind limb ischemia, however, we did not measure skeletal muscle blood flow. To confirm whether this perturbation induced reduction of blood flow and tissue ischemia, we measured dialysate lactate levels in skeletal muscle as an index of tissue ischemia. This perturbation induced increases in dialysate lactate levels. In the present study, dialysate NE responses were examined in prolonged 6 h ischemia. Temporal changes in MAP and HR appeared but sustained significant hemodynamic changes were not observed. This duration was referred to the experiments on the tourniquet application and release time (Sapega et al., 1985; Mitrev et al., 1996). Four to 6 h of ischemic periods has been thought to produce extensive and reversible damage of skeletal muscle. Therefore, data on pharmacological intervention were obtained within 6 h of skeletal muscle ischemia.

Ischemia induced biphasic NE responses in the skeletal muscle. Initial reduction of NE release may be mediated by an impairment of axonal conduction and/or NE releasing function, while in the later phase, the skeletal muscle ischemia-induced NE release was partly attributable to exocytosis via intracellular Ca^{2+} overload rather than opening of calcium channels or carrier mediated outward transport of NE.

Acknowledgements

This study was supported by Grants-in Aid for scientific research (15590787) from the Ministry of Education, Culture, Sports, Science and Technology; the Research Grants for Cardiovascular Disease (H13C-1) from the Ministry of Health, Labor and Welfare.

References

Akiyama, T., Yamazaki, T., Ninomiya, I., 1991. In vivo monitoring of myocardial interstitial norepinephrine by dialysis technique. Am. J. Physiol. 261, H1643–H1647.

Akiyama, T., Yamazaki, T., Ninomiya, I., 1993. Differential regional responses of myocardial interstitial noradrenaline levels to coronary occlusion. Cardiovasc. Res. 27, 817–822.

Akiyama, T., Yamazaki, T., 2001. Myocardial interstitial norepinephrine and dihydroxyphenylglycol levels during ischemia and reperfusion. Cardiovasc. Res. 49, 78–85.

Anton, A.H., Sayer, D.F., 1962. A study of the factors affecting the aluminum oxide-trihydroxyindole procedure for the analysis of catecholamine. J. Pharmacol. Exp. Ther. 138, 360–375.

Barker, D., Saito, M., 1981. Autonomic innervation of receptors and muscle fibers in cat skeletal muscle. Proc. Roy. Soc. Lond., B: Biol. Sci. 212, 317–332.

Cabassi, A., Vinci, S., Quartieri, F., Moschini, L., Borghetti, A., 2001. Norepinephrine uptake is impaired in skeletal muscle of hypertensive rats in vivo. Hypertension 37, 698–702.

Ciuffo, A.A., Ouyang, P., Becker, L.C., Levin, L., Weisfeldt, M.L., 1985. Reduction of sympathetic inotropic response after ischemia in dogs. Contributor to stunned myocardium. J. Clin. Invest. 75, 1504–1509.

Cornett, J.A., Herr, M.D., Gray, K.S., Smith, M.B., Yang, Q.X., Sinoway, L.I., 2000. Ischemic exercise and the muscle metaboreflex. J. Appl. Physiol. 89, 1432–1436.

Cui, J., Wilson, T.E., Shibasaki, M., Hodges, N.A., Grandall, C.G., 2001. Baroreflex modulation of muscle sympathetic nerve activity during postgrip muscle ischemia in human. J. Appl. Physiol. 91, 1679–1686.

Dry, K.L., Phillips, J.H., Dart, A.M., 1991. Catecholamine release from bovine adrenal chromaffin cells during anoxia or metabolic inhibition. Circ. Res. 69, 466–474.

Du, X.-J., Bobik, A., Little, P.J., Esler, M.D., Dart, A.M., 1997. Role of Ca^{2+} in metabolic inhibition-induced norepinephrine release in rat brain synaptosomes. Circ. Res. 80, 179–188.

Fagius, J., Berne, C., 1994. Increase in muscle sympathetic activity in humans after food intake. Clin. Sci. (London) 86, 159–167.

Fern, R., Harrison, P.J., 1994. The relationship between ischaemic conduction failure and conduction velocity in cat myelinated axons. Exp. Physiol. 79, 571–581.

Fujii, T., Kurata, H., Takaoka, M., Muraoka, T., Fujisawa, Y., Shokoji, T., Nishiyama, A., Abe, Y., Matsumura, Y., 2003. The role of renal sympathetic nervous system in the pathogenesis of ischemic acute renal failure. Eur. J. Pharmacol. 481, 241–248.

Hill, J.M., Adreani, C.M., Kaufman, M.P., 1996. Muscle reflex stimulates sympathetic postganglionic efferents innervating triceps surae muscle of cats. Am. J. Physiol. 271, H38–H43.

Idström, J.-P., Soussi, B., Elander, A., Bylund-Fellenius, A.-C., 1990. Purine metabolism after in vivo ischemia and reperfusion in rat skeletal muscle. Am. J. Physiol. 258, H1668–H1673.

Katsuragi, T., Ogawa, S., Furukawa, T., 1994. Contribution of intra- and extracellular Ca^{2+} to noradrenaline exocytosis induced by ouabain and monensin from guinea-pig vas deferens. Br. J. Pharmacol. 113, 795–800.

Kawada, T., Yamazaki, T., Akiyama, T., Sato, T., Shishido, T., Inagaki, M., Tetewaki, T., Yanagiya, Y., Sugimachi, M., Sunagawa, K., 2000. Cyanide intoxication induced exocytotic epinephrine release in rabbit myocardium. J. Auton. Nerv. Syst. 80, 137–141.

Lindsay, T.F., Liauw, S., Romaschin, A.D., Walker, P.M., 1990. The effect of ischemia/reperfusion on adenine nucleotide metabolism and xanthine oxidase production in skeletal muscle. J. Vasc. Surg. 12, 8–15.

Mair, J., 1999. Tissue release of cardiac markers: from physiology to clinical applications. Clin. Chem. Lab. Med. 37, 1077–1084.

Makitie, J., Teravainen, H., 1977. Peripheral nerve injury and recovery after temporary ischemia. Acta Neuropathol. (Berl.) 37, 55–63.

Milusheva, E., Doda, M., Pasztor, E., Lajtha, A., Sershen, H., Vizi, E.S., 1992. Regulatory interactions among axonal terminals affecting the release of different transmitters from rat striatal slices under hypoxic and hypoglycemic conditions. J. Neurochem. 59, 946–952.

Mitrev, Z., Ihnken, K., Poloczek, Y., Hallmann, R., Herold, H., Unkelbach, U., Zimmer, G., Freisleben, H.J., Beyersdorf, S., Beyersdorf, F., 1996. Controlled reperfusion of the extremities for preventing local and systemic damage after prolonged ischemia. An experimental study with the swine model. Zentralbl. Chir. 121, 774–787.

Nukada, H., Dyek, P.J., 1987. Acute ischemia causes axonal stasis, swelling, attenuation and secondary demyelination. Ann. Neurol. 22, 311–318.

Patterson, S., Klenerman, 1979. The effect of pneumatic tourniquets on the ultrastructure of skeletal muscle. J. Bone Joint Surg. Br. 61, 178–183.

Schömig, A., Dart, A.M., Dietz, R., Mayer, E., Kubler, W., 1984. Release of endogenous catecholamines in the ischemic myocardium of the rat. Part A. Locally mediated release. Circ. Res. 55, 689–701.

Schömig, A., Fischer, S., Kurz, T., Richardt, G., Schömig, E., 1987. Non-exocytotic release of endogenous noradrenaline in the ischemic and anoxic rat heart: mechanism and metabolic requirements. Circ. Res. 60, 194–205.

Sapega, A.A., Heppenstall, R.B., Chance, B., Park, Y.S., Sokolow, D., 1985. Optimizing tourniquet application and release times in extremity surgery. A biochemical and ultrastructual study. J. Bone Joint Surg. Am. 67, 303–314.

Tanaka, E., Hattan, N., Ando, K., Ueno, H., Sugio, Y., Mohammed, M.U., Voltchikhina, S.A., Mori, H., 2000. Amelioration of microvascular myocardial ischemia by gene transfer of vascular endothelial growth factor in rabbits. J. Thorac. Cardiovasc. Surg. 120, 720–728.

Thompson, L.P., Mohrman, D.E., 1983. Blood flow and oxygen consumption in skeletal muscle during sympathetic stimulation. Am. J. Physiol. 245, H66–H71.

Tokunaga, N., Yamazaki, T., Akiyama, T., Sano, S., Mori, H., 2003a. In vivo monitoring of norepinephrine and its metabolites in skeletal muscle. Neurochem. Int. 43, 573–580.

Tokunaga, N., Yamazaki, T., Akiyama, T., Sano, S., Mori, H., 2003b. Acute limb ischemia does not facilitate but inhibits norepinephrine release from sympathetic nerve endings in anesthetized rabbit. J. Cardiovasc. Pharmacol. 42, S7–S10.

Toyohara, T., Nada, O., Ikeda, K., 1986. Influence of ischemia on noradrenergic nerves in the terminal colon of humans and rats. Eur. Surg. Res. 18, 349–355.

Turchányi, B., Tóth, B., Rácz, I., Vendégh, Z., Fűrész, J., Hamar, J., 2005. Ischemia reperfusion injury of the skeletal muscle after selective deafferentation. Physiol. Res. 54, 25–31.

Welsh, D.G., Lindinger, M.I., 1993. Energy metabolism and adenine nucleotide degradation in twitch-stimulated rat hindlimb during ischemia-reperfusion. Am. J. Physiol. 264, E655–E661.

Yamada, Y., Teraoka, H., Nakazato, Y., Ohga, A., 1988. Intracellular Ca^{2+} antagonist TMB-8 blocks catecholamine secretion evoked by caffeine and acetylcholine from perfused cat adrenal glands in the absence of extracellular Ca^{2+}. Neurosci. Lett. 90, 338–342.

The EMBO Journal (2006) 25, 2889–2897 | © 2006 European Molecular Biology Organization | All Rights Reserved 0261-4189/06
www.embojournal.org

THE EMBO JOURNAL

Endophilin BAR domain drives membrane curvature by two newly identified structure-based mechanisms

Michitaka Masuda[1,4], Soichi Takeda[2,3,4], Manami Sone[1], Takashi Ohki[1], Hidezo Mori[2], Yuji Kamioka[1] and Naoki Mochizuki[1,*]

[1]Department of Structural Analysis, National Cardiovascular Center Research Institute, Suita, Osaka, Japan, [2]Department of Cardiac Physiology, National Cardiovascular Center Research Institute, Suita, Osaka, Japan and [3]Laboratory of structural biochemistry, RIKEN Harima Institute at SPring-8, Mikazuki-cho, Sayo, Hyogo, Japan

The crescent-shaped BAR (Bin/Amphiphysin/Rvs-homology) domain dimer is a versatile protein module that senses and generates positive membrane curvature. The BAR domain dimer of human endophilin-A1, solved at 3.1 Å, has a unique structure consisting of a pair of helix–loop appendages sprouting out from the crescent. The appendage's short helices form a hydrophobic ridge, which runs across the concave surface at its center. Examining liposome binding and tubulation *in vitro* using purified BAR domain and its mutants indicated that the ridge penetrates into the membrane bilayer and enhances liposome tubulation. BAR domain-expressing cells exhibited marked plasma membrane tubulation *in vivo*. Furthermore, a swinging-arm mutant lost liposome tubulation activity yet retaining liposome binding. These data suggested that the rigid crescent dimer shape is crucial for the tubulation. We here propose that the BAR domain drives membrane curvature by coordinate action of the crescent's scaffold mechanism and the ridge's membrane insertion in addition to membrane binding via amino-terminal amphipathic helix.

The EMBO Journal (2006) 25, 2889–2897. doi:10.1038/sj.emboj.7601176; Published online 8 June 2006
Subject Categories: membranes & transport; structural biology
Keywords: BAR domain; endophilin; liposome; membrane curvature; membrane insertion

Introduction

Membrane dynamics in a cell, such as membrane budding, tubulation, fission and fusion, is associated with changes in membrane curvature. The crystal structure of amphiphysin BAR (Bin/Amphiphysin/Rvs-homology) domain revealed an unexpected structural identity with arfaptin2, a binding protein to Arf and Rac small GTPases (Tarricone *et al*, 2001), and provided a common structural base for the sensing and the formation of positive curvature membrane by BAR-family proteins (Peter *et al*, 2004).

Endophilins are cytoplasmic proteins containing an N-terminal BAR domain and a C-terminal SH3 domain, and are involved in membrane dynamics (Schuske *et al*, 2003; Galli and Haucke, 2004; Wenk and De Camilli, 2004). There are five endophilin genes in the mammalian genomes, endophilin A1–3 and B1–2. Both A and B types are highly conserved from nematode to human. The most extensively studied one is endophilin-A1, a brain specific protein involved in clathrin-mediated synaptic vesicle endocytosis (Ringstad *et al*, 1997, 2001). Via SH3 domain, endophilins bind to the GTPase dynamin, a membrane scissor, and the polyphosphoinositide phosphatase synaptojanin, a clathrin-uncoater (Ringstad *et al*, 1997; de Heuvel *et al*, 1997; Verstreken *et al*, 2003). The BAR domain of endophilins is classified into the N-BAR subgroup characterized by a short amphipathic helical sequence preceding the consensus BAR-domain sequence (Peter *et al*, 2004). The N-BAR domain of endophilin-A1 binds to liposomes and induces the tubulation *in vitro*, requiring the short amphipathic helical sequence (Farsad *et al*, 2001).

The crescent-shaped BAR dimer structure implies a simple model to drive membrane curvature: the dimer may impress its positively charged concave surface on the negatively charged membrane to form a high-curvature membrane domain (Gallop and McMahon, 2005; McMahon and Gallop, 2005). This curvature-impressing or scaffold mechanism for membrane deformation is based on an assumption that the dimer behaves as a rigid body on the membrane (Zimmerberg and Kozlov, 2006). Although the essential requirement of positively charged residues on the concave surface has been suggested (McMahon and Mills, 2004; Peter *et al*, 2004), there have been no experimental supports for the scaffold mechanism. Here, we show the requirement of the molecular rigidity of the BAR dimer for membrane curvature on the basis of structure-oriented mutational analysis.

By determining the structure of endophilin-A1 BAR domain, we found a distinction from those of the known BAR domains: a helix–loop appendage of 30 amino acids stretch is inserted into the helix 1 of the canonical BAR domain. A pair of the helices of the appendages forms a hydrophobic ridge, which runs across the center of the concave surface of the dimer. We analyzed the function of this ridge as well as the previously proposed structure, the N-terminal amphipathic helix and the crescent main body, for membrane deformation (Peter *et al*, 2004). N-terminal amphipathic helix is essential for membrane binding. The crescent main body of the BAR dimer is required for impressing its intrinsic curvature to the membrane. The ridge contributes to deform the membrane

*Corresponding author. Department of Structural Analysis, National Cardiovascular Center Research Institute, 5-7-1 Fujishiro-dai, Suita, Osaka 565-8565, Japan. Tel.: +81 6 6833 5012; Fax: +81 6 6835 5461; E-mail: nmochizu@ri.ncvc.go.jp
[4]These authors contributed equally to this work

Received: 15 November 2005; accepted: 8 May 2006; published online: 8 June 2006

©2006 European Molecular Biology Organization

presumably by penetrating into the membrane. Our results illustrate how these three components coordinate to induce membrane deformation.

Results

Endophilin-A1 BAR domain has a unique appendage

The structure of the BAR domain of human endophilin-A1 (amino acid 1–247, hereafter EndA1-BAR) was solved at 3.1 Å resolution by a multi-wavelength anomalous dispersion method. The structure of EndA1-BAR dimer is similar to that of amphiphysin (Peter *et al*, 2004) and arfaptin2 (Tarricone *et al*, 2001): a crescent-shaped dimer composed of a 6-helix bundle core and two 3-helix bundle arms extended from the core (Figure 1A). The whole structure of EndA1-BAR dimer can be precisely superimposed on that of amphiphysin and arfaptin (Figure 1B). All three structures show nearly identical dimer shapes. Notably, the present EndA1-BAR structure from a tetragonal crystal packing is almost completely the same as an independent crystal structure from an orthogonal crystal packing (Supplementary Figure 1; and Weissenhorn, 2005). The RMS deviations are 0.63, 0.86 and 0.80 Å for Cα atoms in monomers A, B and dimer, respectively. The structural identity indicates that the crescent shape is stably present in solution. Consistent with previous results (Habermann, 2004; Peter *et al*, 2004), structure-based sequence alignment reveals that these three proteins are poorly conserved in amino-acid sequence including the residues possibly important for the crescent-shape formation (Supplementary Figure 2).

We find a unique structure of the EndA1-BAR, an appendage-like structure protruded from the center of the dimer (Figure 1A). The sequence alignments of the BAR-family proteins indicated that this appendage appears unique to the endophilin-family proteins including nadrin (Habermann, 2004; Peter *et al*, 2004) and the candidates from yeasts (Supplementary Figure 2). The appendage (Q59–Q88) has an N-terminal short helix and a loop of which electron density is mostly missing (N72–G85). The pair of helices appears to stay on the main body and forms a ridge across the center of the concave dimer surface. The helix displays, on its top surface, a series of hydrophobic residues (P62, A63, A66 and M70) aligned 60° against the longitudinal axis of the dimer (Figure 1C). Other than the conserved hydrophobic amino acids of the ridge, the appendage sequences show clear distinction between endophilin-A and endophilin-B (Supplementary Figure 2). The B type endophilins show cytoplasmic localization, presumably being involved in intracellular membrane dynamics (Farsad *et al*, 2001; Modregger *et al*, 2003; Karbowski *et al*, 2004). Analyses of chimeric mutations in the appendage between EndA1-BAR and EndB1-BAR suggest that BAR domain may contribute to defining where to target, plasma membrane or intracellular organ membrane (Supplementary Figure 3).

The appendage's penetration enhances liposome tubulation

To investigate the functional significance of the hydrophobic ridge of the endophilin-specific appendage, we first examined the effects of point mutations in this region (red residues in Figure 1C) on the liposome binding and tubulation activities *in vitro* (Figures 2A and 3). Introduction of membrane-repulsive negative charge (A66D) lost the ability to form tubes from liposomes. Hydrophilic mutations (A63S/A66S (SS) and A63S/A66S/M70Q (SSQ)) reduced the number of tubes (<1/100) and induced three-time enlargement of the tube diameter. In contrast, a bulky hydrophobic residue

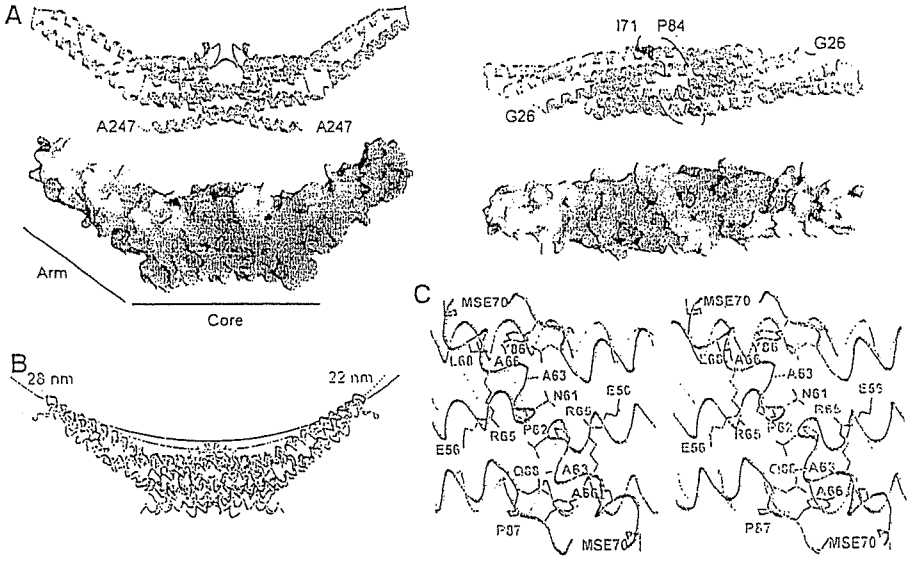

Figure 1 Structure of human endophilin-A1 BAR domain dimer. (A) Ribbon representation (a green monomer with a red appendage and a pale-blue monomer with a blue appendage) and surface electrostatic potential (red, −15 kTe^{-1}; blue, 15 kTe^{-1}) of the dimer viewed from the side (left) and from the top (right). The numbered amino-acid residues are the first and the last ones in consecutive polypeptide segments determined in this model. (B) Comparison of three BAR domain structures in trace representation. Red, endophilin-A1 (PDB ID: 1X03); green, amphiphysin (1URU); blue, arfaptin2 (1I4D). The red and green arcs with indicated diameters represent curved membranes fit the concave surface of endophilin-A1 and amphiphysin, respectively. (C) Stereo view of the appendages. Side-chains of the residues forming the hydrophobic ridge and those of interacting with residues of the main body are shown.

©2006 European Molecular Biology Organization

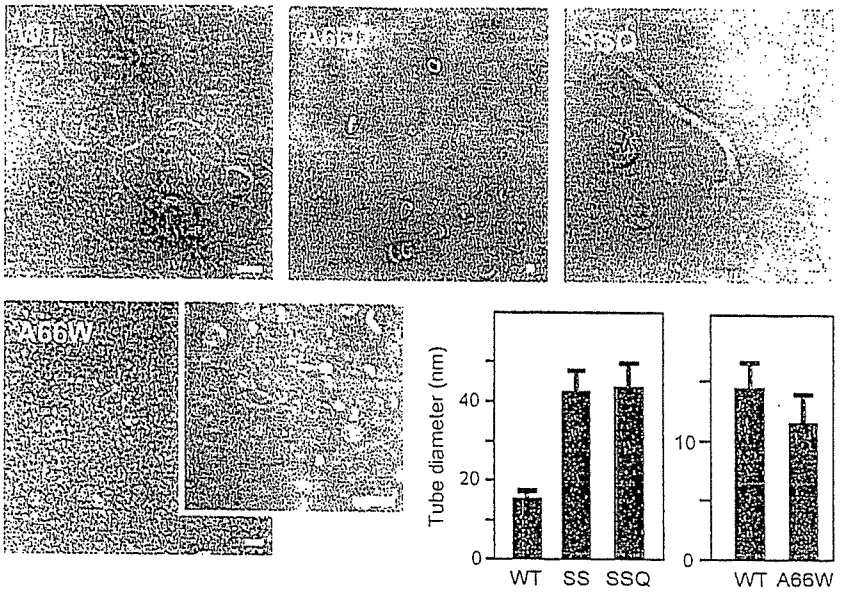

Figure 2 Liposome tubulation by endophilin-A1 BAR domains with mutations in the hydrophobic ridge. WT, 7 μM wild-type BAR domain incubated for 10 min; A66D, 28 μM, 10 min; SSQ, A63S/A66S/M70Q triple mutant, 28 μM, 10 min; A66W, 1.4 μM, 10 min (vesiculated, left panel) and 10 s (tubulated, right panel). Tubulation was not observed when incubated for longer than 1 min. Scale, 100 nm. The bar graphs show tubule diameter (mean and s.d.). SS, A63S/A66S double mutant, 28 μM, 10 min.

Figure 3 Liposome binding assays of endophilin-A1 BAR domain and its mutants. Protein (200 μg/ml) was co-sedimented with liposomes (0, 250 and 750 μg/ml). Proteins recovered from the pellet (p) and the supernatant (s) were analyzed by SDS–PAGE. The DPH-liposomes show similar binding capacity for the wild type (WT) and the A66W mutants. The liposome binding activity is slightly reduced in the F202W and the appendage-less mutants (ΔApp) and is almost lost in the helix 0 truncated mutant (ΔNT).

(A66W) led to extensive vesiculation and less tubulation. All these mutations did not affect the liposome binding. These results suggest an important role for the hydrophobic ridge in the membrane curvature formation but not in the membrane binding.

Although the ridge reduces the intrinsic curvature of the concave surface (red line in Figure 1B), it appears to promote the membrane curvature formation with conserved hydrophobicity. This raises the possibility that the ridge penetrates into the membrane when the concave surface makes tight contact with the membrane. This possibility was investigated using tryptophan fluorescence, which is sensitive to hydrophobicity of the microenvironment around the indole moiety. The A66W mutant showed 10-nm blueshift of the fluorescence peak in a liposome-dose-dependent and saturable manner, while F202W, a control mutant in which Phe202 on the convex surface was mutated to Trp, did not show any shift (Figure 4A and Supplementary Figure 5). The amount of the blueshift was greater than that observed in 50% DMSO or 50% methanol, indicating that the indol moiety was in a highly hydrophobic environment.

To determine whether this blueshift was caused by the insertion of the indol moiety into the hydrophobic core of the lipid bilayer, we made fluorescence resonance energy transfer (FRET) assays using diphenyl-hexatriene (DPH) as the acceptor probe. DPH has been shown to insert specifically in the nonpolar interior of the membrane and not to alter the membrane structure and dynamics (Repáková *et al*, 2005). DPH liposomes did not affect liposome binding and tubulation (Figure 3 and Supplementary Figure 4). A66W but not F202W showed effective FRET from the 340-nm tryptophan fluorescence (donar) to the DPH fluorescence (acceptor) peaked at 430 nm (Figure 4B and C). It was not caused by changes in the fluorescence property of DPH itself possibly accompanied by tubulation/vesiculation of liposomes (Figure 4D and Supplementary Figure 6). These data suggest that the indol ring of 66W penetrates into the hydrophobic core of the membrane and that the remaining residues of the ridge, about 8 Å in height, appear to be embedded in the layer of lipid head-groups of the contacting membrane leaflet. These results confirmed that the ridge is contacting membrane and that the convex is not contacting membrane surface.

To provide further support for the membrane insertion of the ridge in the wild-type EndA1-BAR, we made a mutant

©2006 European Molecular Biology Organization

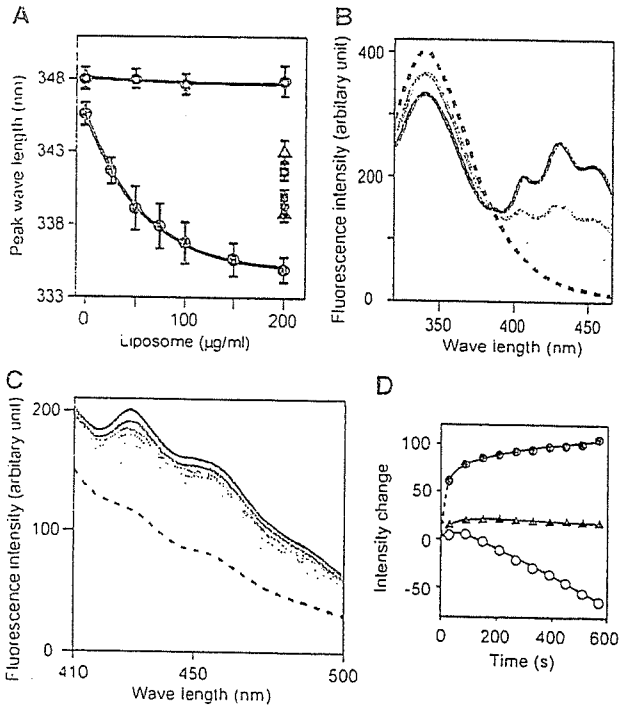

Figure 4 Tryptophan fluorescence blueshift and FRET assays. (A) Tryptophan fluorescence emission peak when excited at 280 nm was observed in different concentration of liposome. A66W (⊕), F202W control mutant (○), A66W alone in 50% DMSO (▲), in 50% MeOH (■), F202W alone in 50% DMSO (△), in 50% MeOH (□), 140 μg/ml protein for all measurements. Mean and s.d. (N=4–11). The dose dependency is significant ($P \ll 0.001$) for the A66W mutant but insignificant ($P > 0.8$) for the F202W mutant (one-way ANOVA). DMSO and MeOH were used as blueshift inducer for tryptophan. (B) Dose-dependent FRET efficiency from the A66W tryptophan to DPH incorporated in liposomes was examined by the changes of fluorescence. Fluorescence spectrum of A66W (100 μg/ml) with the control liposome (200 μg/ml) excited at 280 nm (hatched). Pale to dark solid curves represent DPH:lipid weight ratios of 1:2000, 1:1000 and 1:500 in the same condition. (C) Time-dependent increase in the FRET efficiency from either A66W (pale to dark solid lines, from 30 to 570 s) or F202W tryptophan (pale and dark hatched lines, at 30 and 570 s) to DPH incorporated in liposomes. DPH:lipid weight ratio is 1:500. (D) The intensity changes at the 430-nm peak are plotted against time. A66W (⊕), F202W (▲) excited at 280 nm and A66W (○) excited at 360 nm.

with amphiphysin/arfaptin shape and examined its tubulation activity. The mutant (ΔApp), in which the entire appendage (Q59–Q88) was replaced with a helical stretch (AHLSSLLQ) derived from arfaptin2 sequence (A152–Q159, Y155S), show the crystal structure of a canonical BAR-domain dimer as designed (Figure 5A and Supplementary Figure 7). The ΔApp could bind to liposomes (Figure 3) and cause tubulation to a lesser extent than the wild type and amphiphysin-BAR (Figure 5D and Supplementary Figure 4). As the diameter of the tubules reflects the membrane curvature if the section of the tube is circle, we measured the diameter of the tube to compare the curvature of the EndA1-BAR and its mutant-induced tubes. Despite the higher curvature of the concave surface, the ΔApp dimer induced larger diameter tubules than the wild type did, indicating a positive contribution of the wild-type hydrophobic ridge to drive membrane curvature. Taken all together, the hydrophobic ridge penetrates into the interfacial leaflet of the lipid bilayer when the concave surface is in contact with the membrane and promotes membrane curvature formation

The BAR domain is rigid enough to impose its intrinsic curvature on membrane

A simple model for the concave surface-driven mechanism is that each BAR domain dimer acts as a molecular mold that impresses its curved surface on the membrane. This model suggests that the membrane curvature approximately mirrors the curvature of the concave surface. Indeed, the diameters of tubules induced by amphiphysin, ΔApp (Figure 5D), SS and SSQ mutants (Figure 2) are compatible with the model-based prediction (see Supplementary Table II for statistical analysis). However, this model has an assumption that the dimer should be rigid enough to overcome the bending resistance of the membrane (Nossal and Zimmerberg, 2002; Farsad and De Camilli, 2003). To examine whether the molecular mold mechanism is feasible, we developed a straight BAR domain by inserting one helical pitch into the helix II in the proximal portion of the extending arm (QSAL is inserted between I154 and Q155). This mutation (a4) would compensate the unequal lengths between helix II and III in the arm, a common feature of the known BAR domain structures, and let the curved arm into a straight one. Although the a4 mutant was designed simply to straighten the curvature of the domain, the structure solved at 2.4 Å resolution shows that it actually has the very interesting property of a flexible arm rather than a rigid one (Figure 5B). Four monomers in the asymmetrical unit show deviation in the bending angles of arms. The blue and the green monomers have straight arms while the orange monomer shows a bending pattern similar to the wild type and the yellow monomer is an intermediate. The structural deviation almost exclusively occurs in the helix kink regions (Supplementary Figure 8), indicating that the arm can swing at least from the bend-free straight position to nearly the wild-type position.

The a4 mutant allowed us to examine how flexibility of the crescent-shaped main body of the BAR dimer affects the membrane curvature formation. The insertion of one helical pitch slightly distorts relative position of the helix II and III (Figure 5C), but does not largely rearrange the spatial positions of the residues on the concave surface of the arm (Supplementary Figure 8). Indeed, the a4 mutant and its appendage-lacking derivative (a4ΔApp) retained normal liposome binding activity (Figure 3). The a4 mutant vesiculated liposomes without any tubulation, while a4ΔApp lost these membrane-deforming activities (Figure 5D and Supplementary Figure 4). The concave surface-induced membrane deforming activity appeared to be lost in the a4 mutant, while the appendage's membrane insertion remained active. These results suggested that the rigidity of the crescent dimer structure is essential for liposome tubulation but not for vesiculation, although appendage insertion induces the vesiculation.

Roles for the amphipathic helix 0 of the N-BAR domain

The structure of a short amphipathic helix (helix 0) characterizing the N-BAR (Peter *et al*, 2004) can be resolved in the a4 mutant structure due to its tight crystal packing (Figures 5B and 6). The helix 0 is disordered in the wild type (Figure 6) and the ΔApp structures. The helix 0 has been

©2006 European Molecular Biology Organization

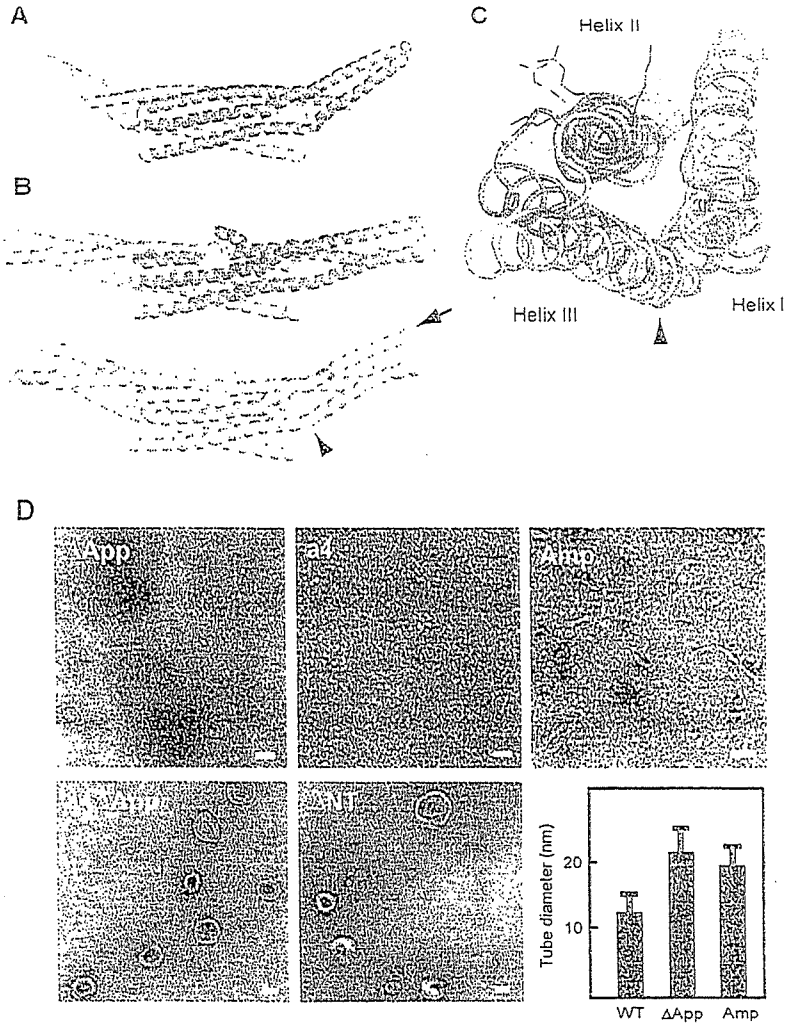

Figure 5 Distinct liposome tubulation induced by endophilin-A1 BAR domain mutants. (A) Ribbon representation of a mutated EndA1-BAR dimer lacking the entire appendages (ΔApp, PDB ID: 1X04). The entire appendage (Q59–Q88) was replaced with a helical stretch (AHLSSLLQ) derived from arfaptin2 sequence (A152–Q159, Y155S). Red, mutated segment. (B) Ribbon representation of the a4 mutant with swinging arms (PDB ID: 2D4C). One helical pitch was inserted into the helix II in the proximal portion of the extending arm (QSAL was inserted between I154 and Q155). Two dimers in the asymmetrical unit are shown separately. Red, inserted segment; magenta, helix 0. The bending patterns of the helix II and III varies among four monomers. An obvious kink in the helix III remains in the orange monomer (arrowhead, also in (C)). The residual curvature in the blue–green dimer is provided by the intersection of the monomers. (C) Superimposition of the a4 mutant monomer (orange one in (B)) and the wild-type monomer (blue) in the core region. A view from the distal end along the helix II (arrow in (B)) shows the maximum structural difference in these arms. Side chains of K171, 173 and R174 are shown. The helix III rotates 12° counterclockwise and shift 6 Å relative to the helix II at the distal end of the arm. The helix 0 and the core region are omitted. (D) Negatively stained liposome tubules induced by the BAR domains of endophilin mutants and amphiphysin. ΔApp, 7 μM, incubated for 10 min; a4, 7 μM, 10 min; a4ΔApp, 28 μM, 10 min; ΔNT, 21 μM, 10 min; Amp, 7 μM, 10 min. Note that a4, a4ΔApp, and ΔNT do not induce liposome tubulation. Scale, 100 nm. The bar graph shows tubule diameter (mean and s.d.).

suggested to be helical only when the amphiphysin BAR domain binds to liposomes (Peter *et al*, 2004). The helix 0 displays the hydrophobic branch of T14, V17 and V21 on one side, while K12, K16 and E19 on the other side (Figure 6). The helix 0 is connecting with the Helix I by a flexible linker G23–G24–A25. Consistent with the previous report (Farsad *et al*, 2001), truncation of the helix 0 (ΔNT) resulted in loss of liposome binding activity (Figure 3) and consequently abolished the tubulation (Figure 5D). In contrast, all the helix 0-containing mutants, including the A66D and the a4ΔApp showed intact liposome binding activity irrespective of their tubulation or vesiculation activities. These results indicate that the helix 0 in the endA1-BAR is critical for liposome binding and that the membrane binding of endA1-BAR via helix 0 is not sufficient to induce tubulation or vesiculation.

BAR domain induces tubular membrane deformation in vivo

To explore the significance of the helix 0, the rigid crescent mold, and the appendage of endophilin-A1 BAR domain *in vivo*, we further examined the membrane deformation activity of endophilin-A1 BAR domain in cells (Figure 7). Human umbirical vascular endothelial cells (HUVECs) expressing endophilin-A1 lacking SH3 domain (residues 1–296, hereafter, EndA1-BAR296), which was C-terminally tagged with enhanced green fluorescence protein (EGFP), exhibited intracellular fibrous structure similar to those induced by other BAR domain-containing molecules (Kamioka *et al*, 2004; Itoh *et al*, 2005). Notably, these structures developed from the periphery toward the center of the cells dynamically and disappeared reversibly in living cells (Figure 7E and

©2006 European Molecular Biology Organization